A longitudinal study to characterize quantitative MRI changes due to progressive formalin-fixation in whole postmortem human brains

by

Anwar Shahadat Shatil

A Thesis submitted to the Faculty of Graduate Studies of

The University of Manitoba

in partial fulfillment of the requirements of the degree of

MASTER OF SCIENCE

Biomedical Engineering

University of Manitoba

Winnipeg, MB, Canada

Abstract

Magnetic resonance imaging (MRI) is an excellent modality to study biological tissue. One of the main advantages of MRI stems from its non-invasive nature and it provides high tissue contrast and spatial resolution, which allow insights into pathology and disease-related alterations in biological tissues. Apart from day-to-day use of MRI in clinical diagnosis, MRI after death (or "postmortem") can be a useful way to obtain images with even higher amount of details to supplement antemortem findings. However, postmortem brain MRI poses three major complications upon removal from the skull. 1) bacteria and autolysis start degrading the brain tissue; 2) air bubbles and air-tissue boundary cause severe image artefacts; and 3) the MR properties change due to tissue fixation, and may not represent the in vivo information.

To overcome these problems, in this thesis, a relatively economical and simple protocol has been introduced, which enables acquisition of artifact-free whole-brain images in typical clinical settings by using formalin as a fixative with minimal death-to-fixation and fixation-to-scan time intervals. Moreover, by using this protocol, different MR properties such as longitudinal relaxation (T_1) and transverse relaxation (T_2), diffusion-based fractional anisotropy (FA), mean diffusivity (MD), and myelin water fraction (MWF) have been measured at thirteen different time points to draw better conclusions about MRI signal changes due to formalin fixation over time. Two neurologically healthy adult female postmortem brains were fixed with 10% phosphate buffered formalin, and four sequences – namely, diffusion tensor imaging (DTI), multi-component T_2-weighted myelin water imaging (MWI), and T_1-weighted magnetization-prepared rapid gradient-echo (MPRAGE) and MP2RAGE sequences – were acquired in each session using a 3T Siemens MRI system. The corresponding FA, MD, T_1, T_2 and MWF maps were processed and evaluated

using four deep white matter (WM) regions of interest (ROIs) (i.e., genu, splenium of corpus callosum, optic radiation, internal capsule) and an additional four gray matter (GM) ROIs (i.e., putamen, thalamus, globus pallidus, caudate nucleus). After plotting the time-course in each ROI at 0, 12, 24, 46, 120, 168, 211, 288, 336, 500, 672, 840 and 1032 hours after initial fixation, it was observed that, FA and MD maps remained fairly constant, whereas T_1 and T_2 appeared to decrease both in WM and GM regions. Interestingly, MWF maps showed increasing trends in all ROIs, with a rapid increase between 46 to 120 hours. These linear changes indicate that formalin gradually diffuses inward from the ventricles and cortical surface, and that tissue fixation continues to affect MR properties until, and perhaps beyond the maximum fixation time of 1032 hours (approximately six weeks) of this study. Although the underlying mechanisms remain ambiguous, the findings suggest that ex vivo T_1-weighted, T_2-weighted and myelin water imaging should be performed soon after tissue fixation (i.e., to avoid erroneous signals), while other factors (e.g., temperature, time between death and fixation, etc.) seem to have additional effects on ex vivo diffusion imaging measures (FA and MD).

By presenting the characteristics and related implications of postmortem ex vivo MRI as a function of formalin fixation, this work has implications for future ex vivo brain imaging studies (both in terms of experimental protocols and data interpretation) and will assist clinicians and researchers to better understand radiology-pathology correlations, brain damage/pathology, and may lead to better imaging strategies to complement regular autopsy practices and improve therapeutic strategies for neurological diseases.

Acknowledgements

I consider myself very lucky and honored to have so many wonderful people leading me through in the accomplishment of this research. First and foremost, I want to express my sincere gratitude to my admirable supervisor, Dr. Chase Figley, for whom I was able to indulge myself in the research of neuroimaging. He has truly been an inspiration for me and I have learned quite a lot from him. He has not only been a superb advisor for my degree at the university, but has also been a great supporter of my ideas. His thoughtful reviews and suggestions during my research and manuscript writings have made my expedition outstanding. I could not ask for more and would like to take this opportunity to say a humble 'Thank you' to you, Chase!

My sincere appreciation to my co-supervisor, Dr. Kant Matsuda who graciously took ample time to listen to my concerns, guide the research and kept me going. Without his support and suggestions, it wouldn't be possible to complete this much.

I also choose this moment to acknowledge the contribution of my committee members, Dr. Zahra Moussavi and Dr. Jennifer Kornelsen, who have provided valuable inputs and constructive feedback throughout the project.

I would like to recognize the funding sources – The University of Manitoba, The Manitoba Graduate Scholarship, The Winnipeg Health Sciences Centre Foundation (HSCF), The Natural Sciences and Engineering Research Council (NSERC) and The Brain Canada Foundation for their continuous financial support.

I would like to take this opportunity to express my gratitude to Teresa Figley who helped me with the figures for my manuscripts and scheduling the scans at the MRI center, and also to my wonderful lab mates Sohail Younas, and Kevin Solar for their time, support and suggestions. I would also like to thank Dr. Md Nasir Uddin for his careful reviews and recommendations during the project and thesis writing.

I would like to recall the assistance of Jennifer Iskierski, Md Amirul Islam, the Biomedical Engineering (BME) academic staffs, BME administrative staffs, University of Manitoba library staffs, MRI Technologists and the Autopsy Technical Assistants at the Winnipeg Health Sciences Centre.

Also, this report, and indeed the completion of this Master of Science, would not have been possible without the love, eternal patience and support of my wonderful family members, especially my wife, Fahmida Rahman, who not only motivated me throughout the thesis, but also, sacrificed a lot during this process.

Finally, but by no means the least, I would like to recognize the continuous motivation and support from my acquaintances in Winnipeg and at the University of Manitoba – an incredible group of people who made my journey an enjoyable one.

Table of Contents

List of Figures

List of Tables

List of Abbreviations

3D	Three Dimension
AD	Alzheimer's Disease
ADC	Apparent Diffusion Co-efficient
BME	Biomedical Engineering
BREB	Biomedical Research Ethics Board
CC	Corpus Callosum
CNR	Contrast-to-Noise Ratio
CNS	Central Nervous System
CSF	Cerebrospinal Fluid
DTI	Diffusion Tensor Imaging
EPI	Echo Planar Imaging
ESP	Echo Spacing
ETL	Echo Train Length
FA	Fractional Anisotropy
FDT	Fit Diffusion Tensor
FMRIB	Oxford Centre for Functional MRI of the Brain
FOV	Field Of View
FSL	FMRIB software library
GCC	Genu of Corpus Callosum
GD-dTPA	Gadolinium- di-ethylene Tri-amine Penta-acetic Acid
GM	Gray Matter

GP	Globus Pallidus
GRASE	Gradient and Spin Echo
HARDI	High Angular Resolution Diffusion Imaging
IC	Internal Capsule
ICBM	International Consortium for Brain Mapping
IRE	Image Reconstruction Environment
JHU	Johns Hopkins University
LDDMM	Large Deformation Diffeomorphic Metric Mapping
MD	Mean Diffusivity
MET_2	Multi-Exponential T_2
MIPAV	Medical Image Processing, Analysis, and Visualization
MNI	Montreal Neurological Institute
MP2RAGE	Magnetization-Prepared Rapid Gradient-Echo 2
MPRAGE	Magnetization-Prepared Rapid Gradient-Echo
MRI	Magnetic Resonance Imaging
MS	Multiple Sclerosis
MSDS	Material Safety Data Sheets
MTI	Magnetization Transfer Imaging
MTR	Magnetization Transfer Ratio
MWF	Myelin Water Fraction
MWI	Myelin Water Imaging
NNLS	Non-Negative Least Squares

OR	Optic Radiation
PBS	Phosphate Buffered Solution
PD	Proton Density
PMI	Postmortem Interval
Put	Putamen
RF	Radio Frequency
ROI	Region of Interest
SCC	Splenium of Corpus Callosum
SE-EPI	Spin Echo – Echo Planar Imaging
SI	Scan Interval
SNR	Signal-to-Noise Ratio
SPM12	Statistical Parametric Mapping 12
TE	Echo Time
TE1	First Echo Time
TH	Thalamus
TI	Inversion Time
TR	Repetition Time
UK	United Kingdom
WM	White Matter

Chapter 1 : Introduction

1.1 Thesis overview

This thesis has been compiled in “sandwich” style. It consists of two research articles (one already published, and one that is currently under review) bound by General Introduction and General Discussion chapters. The introduction chapter briefly discusses the key concepts of MRI and motivates the thesis by defining the main objectives. The second chapter covers the methodology of the study, which describes the overall process from sample procurement to image acquisition, and has already been published in *Frontiers in Neurology* (1). Chapter 3 describes the results of the study and also includes the image processing steps that were used. A version of this chapter has been submitted in *Magnetic Resonance in Medicine* and is currently under review. In the last chapter, the thesis is concluded, where a general discussion about the project and some insights on future routes have been portrayed. All the references have been put together at the end of the thesis.

1.2 Basic MRI Physics: A brief overview

There exist a number of resources describing the underlying concepts of MRI. However, most of the information in this chapter has been summarized based on the textbook by Prasad, 2006 (2).

Before going more into the details of advanced MRI techniques, it is required to refresh some knowledge of basic MRI physics. There are three basic stages in an MRI experiment e.g., 1) preparation of nuclear magnetic system, 2) excitation of the nuclear magnetic system, and 3) acquisition of signal from the excited nuclear magnetic system before it relaxes back to its thermal equilibrium state. However, the exact theory of MRI lies in quantum mechanics. Every human body comprises water molecules, and each water molecule contains two hydrogen atoms (or proton), which have intrinsic spin property. Each proton can be considered as a small bar magnet that creates a magnetic field by rotating about its own axis, just like a gyroscope. When a person is placed inside a powerful magnetic field (B_0) of the MRI scanner (e.g., magnetic field of 3T MRI scanner is 60,000 times stronger than earth's magnetic field), the protons start to precess about the field's direction, thus creating a magnetic moment. This precession can be visualized by a spinning top with a little wobble about the vertical due to gravitation. The frequency of this precession is named essentially as Larmor frequency, ω_L, which is directly proportional to the applied magnetic field. Although, all the protons of a specific tissue do not precess in the same direction, but a significant amount of protons precess parallel to the direction of external magnetic field, rest being antiparallel. This precession causes a net magnetic field (the vector sum of each tiny magnetic moment in the longitudinal direction, known as nuclear magnetization or magnetization, denoted as M_0) in tissue volume, but not enough for a detectable MR signal. In order to excite or perturb the spin system, an 'oscillating' magnetic field (B_1) perpendicular to the static field (B_0) is applied that possesses the same frequency as the resonant (Larmor) frequency of the precessing protons. This condition, written as $\omega_{RF} = \omega_L$, is called Radio Frequency (RF) excitation, because Larmor frequency falls within the range of radio frequencies. The RF excitation causes the net magnetization to tip away from the longitudinal axis into the transverse plane. Then, after the RF

pulse, the net magnetization returns to its previous thermal equilibrium state by re-aligning with the main magnetic field B_0. This process is called relaxation. During the relaxation process, an RF signal is generated which can be measured using receive coils and translated into image. However, signal localization is necessary for selective excitation of the spin (i.e., spinning proton) in a subject, which can be achieved (i.e., specific slices can be selected) by superimposing additional spatially varying magnetic fields (or gradients) onto the main magnetic field (B_0) making resonance frequency as a function of position. Each MRI scanner has 3 sets of gradient coils to produce spatially varying magnetic fields in the three orthogonal directions (x, y and z) and signal localization can be achieved by using 3 methods such as slice selection, frequency encoding and phase encoding. The final MRI image can be obtained by Fourier transformation of the spatial frequencies of the signal.

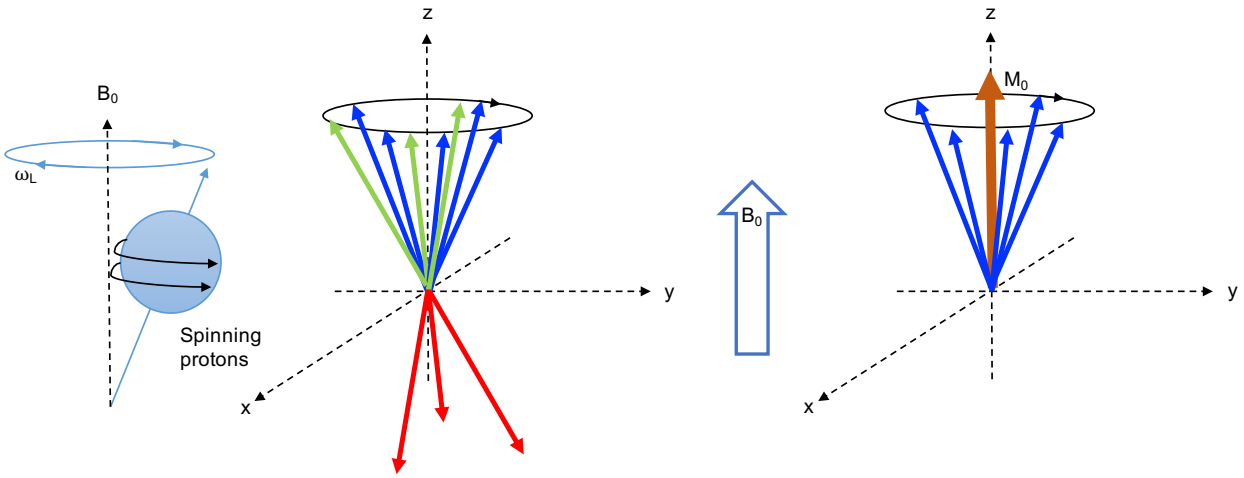

Figure 1-1: *Protons rotate on its own axis and upon an external parallel field it starts to precess like a spinning top with a little wobble. Protons pointing in opposite direction (red arrows) cancel each other's magnetic effects (green arrows). The remaining protons (blue arrows) create a Net magnetization (M_0) parallel to the external field (B_0).*

1.3 Relaxation mechanism

So far, we have come to know that, an RF pulse makes the spins precess synchronously, which produces a detectable rotating magnetic field. However, once the external (RF) energy is removed, transverse magnetization will be lost – and this is called "relaxation," which occurs via two mechanisms (described below).

1.3.1 Longitudinal (T_1) relaxation

To better understand relaxation, let us consider a three dimensional frame having x, y and z axes (Figure 1-1). As mentioned earlier, when only a longitudinal external field B_0 is applied, the net magnetization vector remains at equilibrium, parallel to B_0 (say at +z direction), and is referred to as equilibrium magnetization, M_0. In this setting, there is only a z component of magnetization (M_z) and no magnetization component exists along the x or y axis. This M_z component is called "longitudinal magnetization." Upon application of a 90° RF pulse (B_1), transitions between lower to higher energy states are induced. As a result, the net energy of protons becomes higher than its equilibrium value and they start to precess in xy plane, so that the resultant magnetization M_z becomes zero (Figure 1-2). After removing the RF pulse, M_z returns to its previous state (reaching $M_z = M_0$) as the protons lose their absorbed energy to their surroundings (tissue lattice) and want to restore their previous low energy state, i.e. precessing in +z axis. This process, where transverse magnetization is lost as longitudinal magnetization is restored, is known as longitudinal relaxation or spin-lattice relaxation and the time taken by the protons to restore the longitudinal magnetization (63% restoration to be exact) is called the T_1-relaxation time – and importantly, this property is different for various types of tissues.

This relaxation can be shown as:

$$M_z = M_0\,(1 - \ e^{-\frac{t}{T_1}})$$

The T_1-relaxation not only depends on the type of molecule in which it is bound, but also on the surrounding environment (i.e. the type of tissue) in which it is present. For example, free (unbound) water or body fluids like cerebrospinal fluid or blood have longer T_1 than water bound in tissues like gray matter or white matter in the brain. Using the differences in T_1 values among tissues, different intensities can be achieved on MR images. While acquiring MRI of any tissue, RF pulses are applied not once, but many times in quick succession. The time between successive RF pulses is called the repetition time, TR; and different amounts of T_1-weighting can be achieved by increasing (less T_1-weighting) or decreasing (more T_1-weighting) the TR.

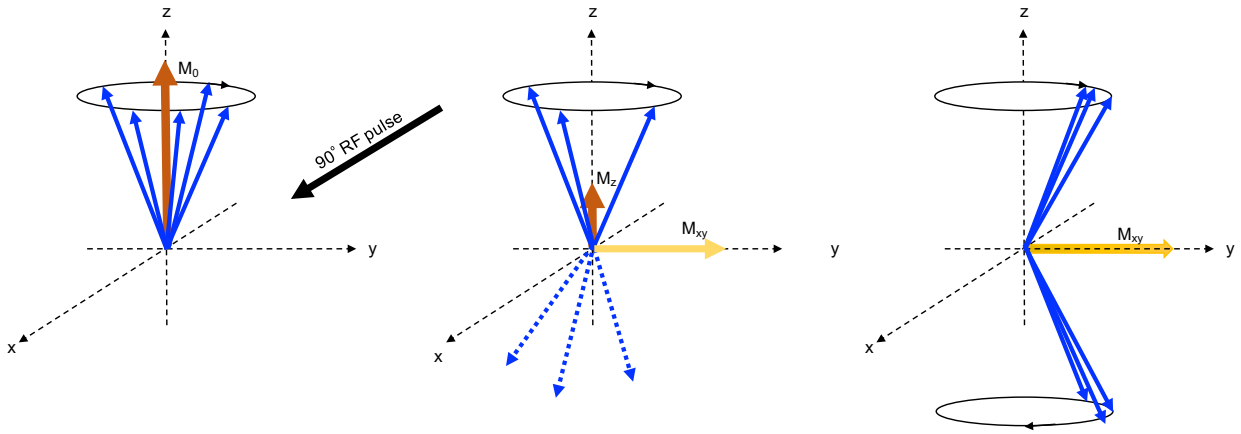

Figure 1-2: *The 90^0 RF pulse has two effects on protons: it tips some protons to higher energy level and also makes them precess in phase. The former causes a decrease in longitudinal magnetization and the latter establishes transverse magnetization in xy plane.*

1.3.2 Transverse (T_2) relaxation

However, in addition to longitudinal (T_1) relaxation there is also a second mechanism through which net transverse magnetization is lost after removing the 90° RF pulse. It happens simultaneously with spin-lattice relaxation, but happens so rapidly that the signal needs to be detected during that short period. At a relatively long excitatory 90° RF pulse, the spins start to precess in-phase (same phase) and create a net magnetization vector in xy plane by losing their longitudinal magnetization (Figure 1-2). Because all spins are in-phase, the vectors of their individual tiny magnetizations exhibit same direction, which in total is called transverse magnetization, M_{xy} (M_0 equaling to M_{xy}). However, at the end of this RF pulse, the protons lose their phase coherence due to energy transfers among neighboring protons and magnetic inhomogeneities of external field, B_0. As a result, the individual tiny magnetization vectors of protons influence each other and start precessing at different phases. Eventually, they start to de-phase and transverse magnetization gradually reaches to zero. This process of getting out-of-phase from an in-phase situation is known as transverse relaxation or spin-spin relaxation. The time taken for this relaxation (at least 37% of de-phasing) to happen is denoted as T_2. It can be measured by following equation:

$$M_{xy} = M_{xy}\, e^{-\frac{t}{T_2}}$$

The value of T_2 can be smaller than T_1 and it depends on the binding of protons with the surrounding and the type of tissue. The time between excitation pulse and MR signal collection is referred to as echo time, TE, which is exactly the sum of time allowing for dephase and rephase. By varying echo time, one can obtain images with different T_2 contrasts. Figure 1-3 shows the decay of T_1 and T_2 relaxations over time.

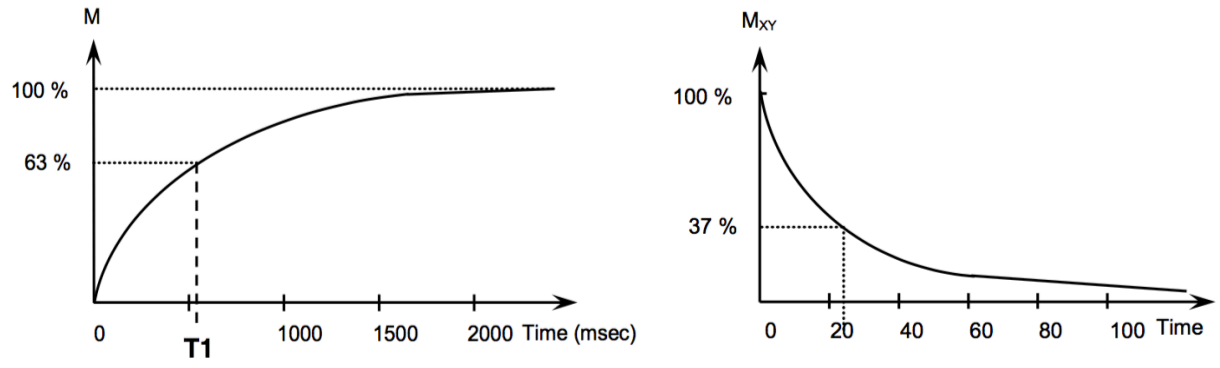

Figure 1-3: *The decline of T_1 and T_2 relaxations.*

1.4 T_1-weighted and T_2-weighted imaging

By varying TE and TR, different types of image contrast can be achieved. If the TR is kept shorter (and TE << TR) than the T_1 of the tissue, then the protons do not get enough time to fully recover their longitudinal magnetization, thus resulting a saturated magnetization and a reduced MR signal. Generally, the degree of recovery follows the factor of $e^{-TR/T1}$ and if TR is very short, then the signal from the tissue relies heavily on its T_1 relaxation. Thus a T_1- weighted image is created. T_1 weighted images are typically useful to present anatomical structures (fat appears bright and fluid appears dark) and also suitable for image segmentation and for creating anatomical brain masks. However, MR sensitive contrast agents such as Gadolinium- diethylenetriaminepentaacetic acid (Gd-DTPA) also appears bright in T_1 weighted images (because of its T_1 shortening effect) after injecting in the brain, which is a common practice to clinically study hypervascularity and related pathology.

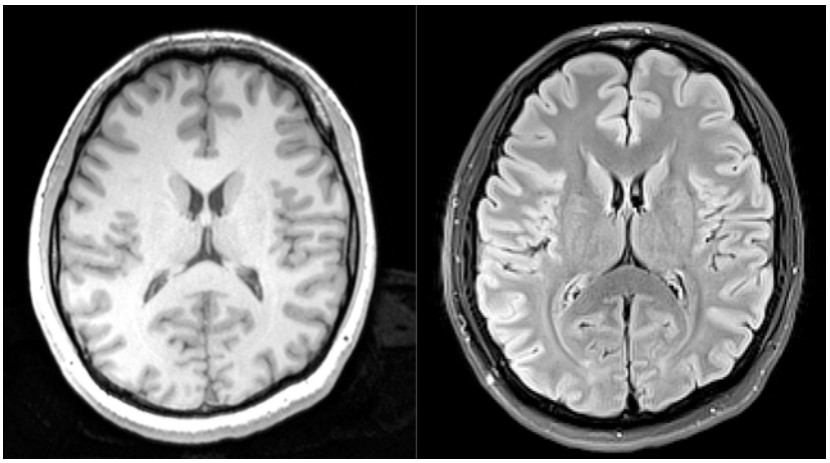

Figure 1-4: *Example of T_1-weighted (on the left) and T_2-weighted (on the right) images of a healthy subject.*

In contrast, if the TR is long, then TE can be made of dominant factor to exhibit an image contrast and this is known as T_2-weighted image. Typically, white matter lesions look hyper-intense on T_2-weighted images and are, therefore, preferred for studying tissue pathology such as tumor, edema, inflammation, infarction, etc., which provide bright signal.

1.5 Diffusion Tensor Imaging (DTI)

1.5.1 Diffusion and diffusion tensor

Diffusion is the random molecular motion in a medium that is caused due to thermal energy of molecules. Human body weight is made up of 60-80% water. The heat generated by the body energizes the water molecule and thus the molecules move randomly. This phenomenon was first described by Robert Brown (3) and is known as 'Brownian Motion.' In an undamaged tissue, cell membranes control the nature of diffusion, whereas, an increased diffusivity is a sign of tissue disruption. As a result, diffusion is a useful way to identify certain lesions or degenerative

alterations in the tissue. Also, by assessing the direction of water diffusion, it is possible to infer tissue integrity and the trajectories of white matter tracts in the brain.

In tissue fibers (such as white matter), water diffusion follows the direction of fiber tract orientation. Likewise, diffusion is highly obstructed in the orthogonal directions of the fibers. This idea of parallel and perpendicular diffusion was used in the early 1990s (4,5) to explain diffusion anisotropy. Later in 1994, the tensor model was introduced to characterize anisotropic diffusion in detail (6,7). Diffusion tensor, D is presented as a 3 x 3 covariance matrix as follows,

$$D = \begin{bmatrix} D_{xx} & D_{xy} & D_{xz} \\ D_{yx} & D_{yy} & D_{yz} \\ D_{zx} & D_{zy} & D_{zz} \end{bmatrix}$$

It represents the covariance of diffusion displacement in a three dimensional system. The xx, yy and zz elements are the diffusion variances in x, y, z axes respectively and the rest of the elements describe the covariance. This diagonal model (Figure 1-5) introduces three eigenvalues (λ_1, λ_2, λ_3) and three corresponding eigenvectors ($\hat{e}_1$, $\hat{e}_2$, $\hat{e}_3$), which provide the degree of apparent diffusion and directions along the axes.

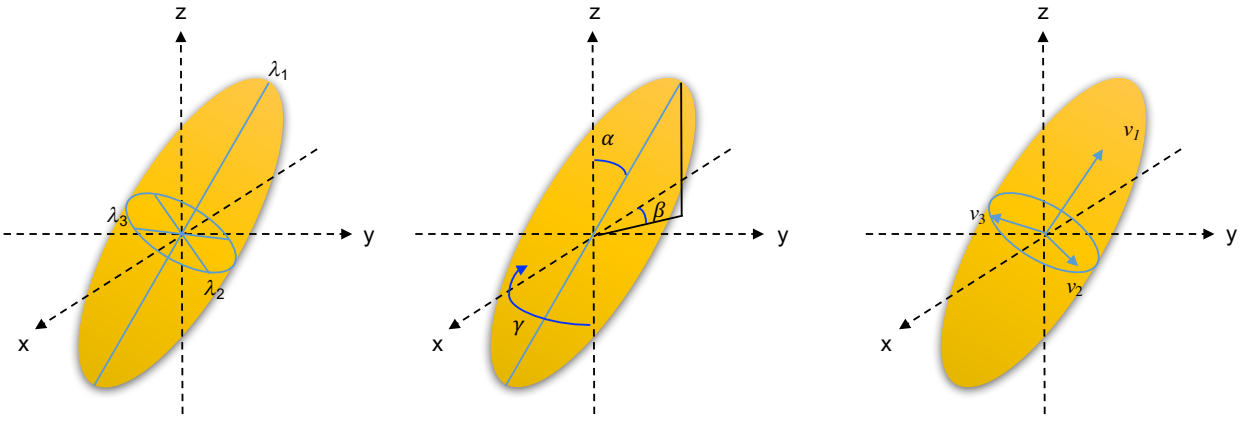

Figure 1-5: *Six parameters are required to define a tensor ellipsoid in three dimension.*

In summary, the diffusion tensor may be pictured as an ellipsoid having three radii in three directions, which are described by these eigenvalues and eigenvectors. If the eigenvalues are close to equal then diffusion is said to be isotropic (i.e., the same in all directions) and if the eigenvectors have significantly different magnitudes, then diffusion is said to be anisotropic (i.e., directionally dependent). For example, in the central nervous system (CNS), cerebrospinal fluid (CSF) diffusion is unrestricted and isotropic (directionally-independent), whereas diffusion in white matter is restricted and anisotropic (directionally-dependent) along the axon fibers (8–10). Thus, DTI is sensitive to water diffusion and can provide valuable information about tissue microstructures and fiber orientation.

1.5.2 Mean diffusivity

To quantify diffusion properties, two scalar maps are widely used. One is called mean diffusivity (MD) and another is fractional anisotropy (FA). The sum of the three eigenvalues or diagonal elements (D_{xx}, $D_{yy,}$, D_{zz}) is called the 'Trace' and by averaging these eigenvalues, mean diffusivity is achieved, as shown by,

$$MD = \frac{\lambda_1 + \lambda_2 + \lambda_3}{3} = \frac{D_{xx} + D_{yy} + D_{zz}}{3} = \frac{Trace}{3}$$

MD explains the average rate of molecular diffusion, such that higher values of MD correspond to higher diffusivity and vice versa.

1.5.3 Fractional anisotropy

Another way to quantify diffusion is to calculate the degree of diffusion anisotropy, which is called fractional anisotropy (FA). FA values are relative measures that range from 0 (meaning isotropic diffusion) and 1 (meaning anisotropic diffusion), and are calculated by following equation (11),

$$FA = \sqrt{\frac{3}{2}}\sqrt{\frac{(\lambda_1 - MD)^2 + (\lambda_2 - MD)^2 + (\lambda_3 - MD)^2}{{\lambda_1}^2 + {\lambda_2}^2 + {\lambda_3}^2}}$$

Although, FA does not provide any information about fiber orientation and does not vary with fiber rotation, FA can be combined with the vector information to create color-coded maps that show the diffusion magnitude and directionality.

A sample image from each of FA and MD maps have been shown in Figure 1-6.

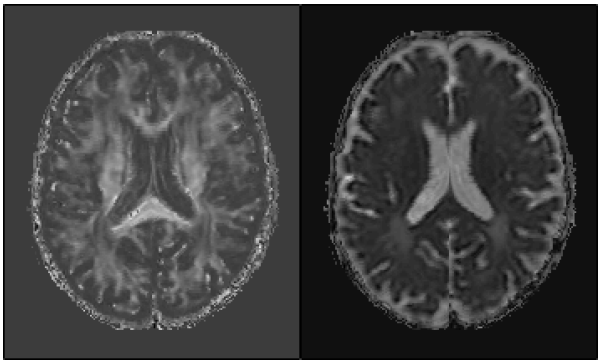

Figure 1-6: *Sample FA (left) and MD (right) maps showing tissue contrasts related to different diffusion characteristics.*

1.5.4 Application of DTI measurements

Due to its ability to provide sensitive information on tissue microstructure as well as fiber orientations, DTI has become a common clinical and research tool for detecting and studying a variety of brain abnormalities (12,13). It has been successfully applied to study brain tumors or acute strokes; neurodegenerative diseases such as Alzheimer's, MS, and epilepsy; schizophrenia; autism; dyslexia; Huntington's; Parkinson's; Williams syndrome; fragile X syndrome; and in neurodevelopmental changes (12,14–27). DTI measures such as FA can provide information on alteration in myelination and axonal injury (9,28–30). A postmortem MS study has revealed that

MD and FA has univariate correlation with myelin and axonal contents and can be used as an MS marker (31). Although in vivo DTI is much more common, ex vivo DTI studies are also being conducted both in animal and human brains (31–42) and revealing interesting facts. With an increasing range of applications, robustness of the method and reliability of results, it is expected that DTI will be valuable in planning the treatments and detection of diseases and microstructural abnormalities in the future.

1.6 Myelin Water Imaging

1.6.1 Myelin

Myelin is an essential component of the central nervous system. It is well known that myelin is responsible for the fast and efficient transmission of action potentials throughout the brain. During early neurodevelopmental stages, the degree of myelination is increased. However, there are a number of neurodegenerative diseases where myelin integrity is reduced (i.e., Multiple Sclerosis, Alzheimer's Disease, etc.). As a result, a specific myelin measurement is important to understand brain plasticity and brain damages.

The aqueous portion (70-80%) of the brain contains water (including intracellular and extracellular pools), whereas the rest consists of non-aqueous components such as proteins, lipids and nucleic acids. The membranes of most glial cells and unmyelinated neurons are made of a single bilayer, whereas axons of myelinated neurons are ensheathed by multiple layers of oligodendrocyte membranes, which contain 40% of total water in brain.

1.6.2 Myelin water fraction

Unfortunately, direct MRI measurements of the non-aqueous protons of myelin (i.e. protons in myelin lipid and protein) is almost impossible due to two reasons: (a) they have less mobility, hence, very short T_2 (10 μs < T_2 < 1 ms) and (b) MR signal from the protons of other non-aqueous components of CNS make myelin proteins and lipids almost indistinguishable (43). Although, use of ultrashort TE (44) could be one possible approach, the difficulties associated with removal of unwanted water signals make this technique unadoptable in clinical use. However, to date, several other indirect approaches have been investigated such as conventional T_2-weighted imaging, DTI, magnetization transfer imaging (MTI) and multi-exponential T_2 (MET_2) imaging. But none of them has been proven to be a valid (sensitive and specific) measure of myelin except MET_2. It has been reported that gliosis (proliferation of glial cells), inflammation (proliferation of inflammatory cells), loss of axons (axonal breakdown), demyelination (breaking of myelin sheath) and edema (increment of intra- and extra-cellular water) cause changes in T_2 signal intensities (45), thus, T_2 weighted imaging is less specific to myelin. DTI can provide information on the "changes" in myelination, but it is unreliable in providing exact information on myelin (46) because of the high dependency of the diffusion tensors on fiber tract orientations and membrane densities in particular image voxels. In addition, it has been previously reported that having a diffusion anisotropy in nerve fibers might not necessarily mean the existence of myelin (47). In MTI, the exchange of magnetization between water and tissue fibers are measured in the form of magnetization transfer ratio (MTR) (48). MTR has been proven to have very high sensitivity to tissue damage but an MS study has reported that inflammation can affect MTR (49). Therefore, MTR cannot be considered as a valid measure of myelination. MET_2, on the other hand, measures the water trapped between myelin bilayers. In this method, images are acquired at multiple TEs and T_2-relaxation curves are

analyzed. In 1994, such analysis in CNS tissue in vivo revealed two distinguishable water components (50) : short T_2 component (~20ms) from water trapped in myelin sheath and intermediate T_2 component (70 ~100ms) from intra- and extra-cellular water. A third component was also observed which had longer T_2 (>1s) and arose from cerebrospinal fluid. By measuring the ratio of signal area of short T_2 distribution (10 ms < T_2 < 50 ms) to the area of total T_2 distribution, myelin water fraction (MWF) can be measured (Figure 1-7). Previous MRI-histopathology correlation studies in rat sciatic nerve (51) and postmortem MS subjects (52,53) led to accept MWF as a marker of myelin integrity. Therefore, MWF can be portrayed visually by myelin water imaging (MWI). The major challenge of MWI sequences is minimizing the scan time so that it can be performed in acceptable clinical scan time.

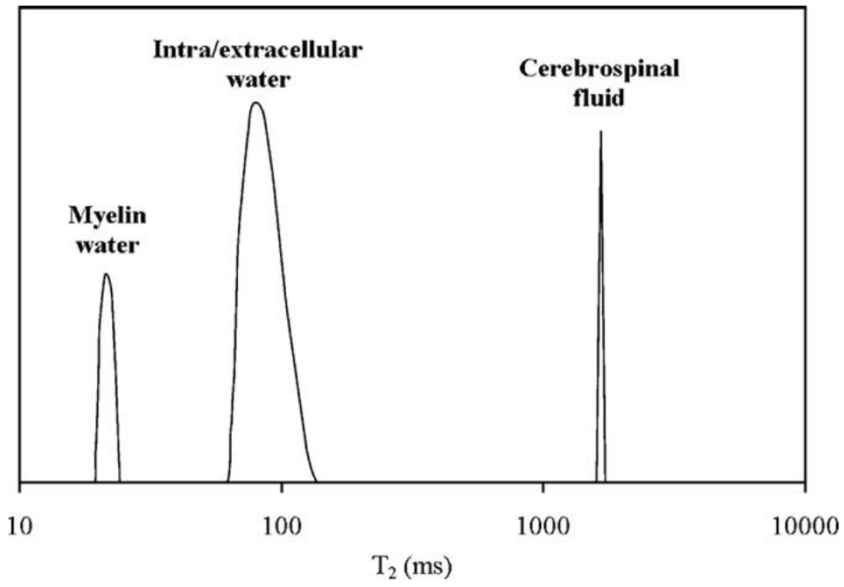

Figure 1-7: *Non-negative least squares (NNLS) fitting can be used to extract different components from the overall T_2 relaxation curves obtained from human brain tissue. The resulting T_2 distributions are associated with myelin water (short relaxation component), intracellular and extracellular water (intermediate relaxation component), and cerebrospinal fluid (long relaxation component). Reproduced with permission from McKay et al. (54) (See Appendix A)*

1.6.3 T_2 decay curve analysis

One important aspect of myelin water imaging is T_2 decay curve analysis. Figure 1-8 represents the differences in T_2 decay curves in human white matter, grey matter and cerebrospinal fluids. From these semi-logarithmic T_2 plots, it is evident that the T_2 decay rate is different between WM and GM structures. Moreover, these curves cannot be fitted by a single straight line, which indicates that these regions can contain several water environments, each having its own distinguishable T_2 time. As a result, a fitting algorithm is used to estimate the number of exponentials. The most common approach is non-negative least squares (NNLS), which produces few discrete spikes of T_2 components (55,56) and uses χ^2 minimizing algorithm with a regularizer component (i.e. the energy of T_2 distribution). By minimizing both χ^2 and regularizer, a smoother T_2 distribution is achieved and thus the T_2 decay curve is fitted. An example of NNLS fitting of T_2 distribution of human white matter in vivo is shown in Figure 1-7, which illustrates the short, intermediate and long T_2 components mentioned in section 1.6.2.

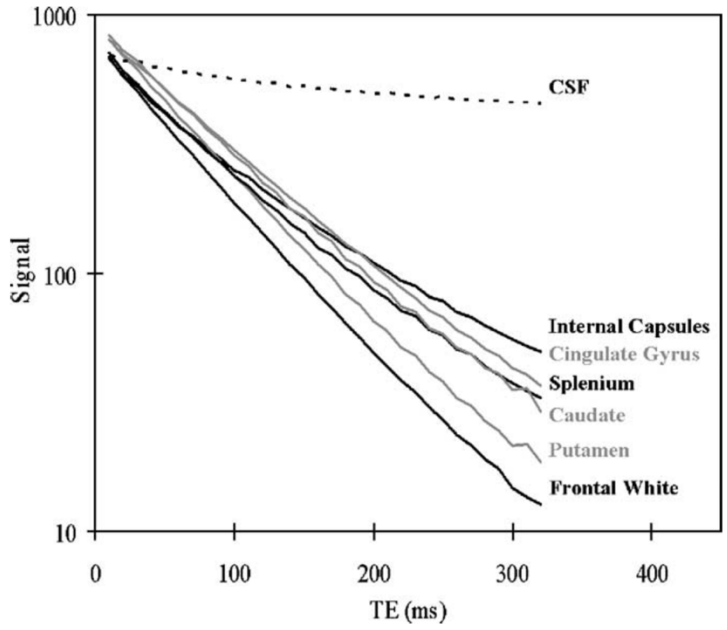

Figure 1-8: *White matter, grey matter and cerebrospinal fluids have different T_2 decay curves. Reproduced with permission from McKay et al. (54) (See Appendix A)*

1.6.4 Application of MWF

As stated in the previous section, MWI-based myelin water fraction (MWF) can assess white matter myelination (57), and there have been several in vivo studies where MWF has been effectively used to understand neurological diseases such as MS (50,57,58), Alzheimer's disease (AD) (59), schizophrenia (60), and phenylketonuria (61). A few ex vivo studies were able to validate MWF histopathologically as a marker of myelin integrity in brains with multiple sclerosis (52,53,62,63). However, further studies are still being conducted and it is expected that, MWF will be one of the MR measures to reliably detect white matter diseases in the future.

1.7 MRI of postmortem brain

Although in vivo scanning gives good quality images, obtaining brain slices from a living human body are inconceivable and thus it is difficult to study at the cellular-molecular level. Likewise, for higher resolution three-dimensional (3D) imaging, long scan times and large numbers of images are often required. This puts excessive stress on the patient to remain still for relatively long durations. As a result, for validating fine tracts or small tract features, imaging *postmortem* human brains by various MRI techniques (DWI, DTI, MTI, MWI etc.) has been another option (36,39,40,64–67). Postmortem tissue provides the benefits of having no motion artifact, no time limit and no restriction to image numbers, which in turn gives images with higher spatial resolution and higher signal to noise ratio (SNR). Moreover, it reduces image artifacts due to air-tissue interfaces (e.g., near the sinuses and auditory canals) and defective shim arising from magnetic field inhomogeneity (40). Several studies have been conducted on animal brains using pre-clinical scanners with ultra-high magnetic field strengths (7T or above) and small bores (32–36,38,68). However, animal models are often limited, particularly in cases involving distinctively human pathologies such as MS or psychiatric disorders (39). Usually animal scanners give the advantage of high performance gradients, which enables stronger diffusion-encoding (i.e., higher b-value) with short echo time (TE) and high resolution images. But unfortunately, due to its large size, postmortem human brains are not possible to place in those scanners and that leaves the researchers with the only option of using clinical scanners and at conventional field strengths (1.5T or 3T).

Traditional autopsies are invasive in nature, but they can verify antemortem status, provide disease specific mortality data and help in exact counseling about recurrence possibility for other family members (69,70). With regards to non-invasive autopsy, postmortem MRI is more welcoming to

parents and next of kin than usual intrusive autopsy procedures (71,72). Moreover, MRI based death certificates are being accepted in some UK health centers (73). However, the recognition of postmortem MRI as an alternative to regular autopsy is not yet approved in most of the healthcare providers throughout the world due to lack of precision. Therefore, a more accurate validation is required for postmortem MRI in human brains.

1.8 Thesis Motivation

After removing the brain from the skull, bacteria and autolysis make postmortem tissue susceptible to degradation; thus, chemical fixatives are required to preserve the tissue (35). Moreover, air-bubbles and air-tissue boundaries in the brain introduce magnetic susceptibility that worsens the image quality. Although, there are a handful of fixatives, formalin also known as formaldehyde, is the most common one used in pathology labs, because it is easier to remove from the cortical surface and good for brain fixation and/or histological staining (74–76). However, fixatives alter MRI signals, and this is a major challenge for postmortem MRI. Moreover, no previous studies have presented an artefact-free, cost-effective and clinically acceptable technique to conduct whole-brain longitudinal ex vivo studies by continuous immersion in formalin, nor they have characterized formalin changes of different MR properties (including MWF) in a longitudinal manner. Thus, the potentials of using postmortem MRI in future studies as a medium of tracking antemortem status during autopsy or as a “biomarker” have remained an area of need.

1.9 Thesis Objectives

Therefore, this thesis has two major aims, which have been addressed in the following chapters:

1. To develop an affordable and clinically-acceptable fixation method which will facilitate the acquisition of artefact-free MR images of whole postmortem human brains and,
2. To find a correlation between prolonged formalin fixation and different MR properties (i.e., FA, MD, T_1, T_2, and MWF) that will explain possible implications for future postmortem studies.

Chapter 2 : A Method for Whole Brain Ex vivo Magnetic Resonance Imaging with Minimal Susceptibility Artifacts

2.1 Abstract

Magnetic resonance imaging (MRI) is a non-destructive technique that is capable of localizing pathologies and assessing other anatomical features (e.g., tissue volume, microstructure, white matter connectivity) in postmortem, ex vivo human brains. However, when brains are removed from the skull and cerebrospinal fluid (i.e., their normal in vivo magnetic environment), air bubbles and air-tissue interfaces typically cause magnetic susceptibility artifacts that severely degrade the quality of ex vivo MRI data. In this report, we describe a relatively simple and cost-effective experimental set-up for acquiring artifact-free ex vivo brain images using a clinical MRI system with standard hardware. In particular, we outline the necessary steps, from collecting an ex vivo human brain to the MRI scanner setup, and have also described changing the formalin (as might be necessary in longitudinal postmortem studies). Finally, we share some representative ex vivo MRI images that have been acquired using the proposed setup in order to demonstrate the efficacy of this approach. We hope that this protocol will provide both clinicians and researchers with a straight-forward and cost-effective solution for acquiring ex vivo MRI data from whole postmortem human brains.

2.2 Introduction

Magnetic resonance imaging (MRI) has become one of the most commonly used medical imaging modalities among human neuroscientists due to its ability to non-invasively visualize and quantify various anatomical and microstructural characteristics of the brain. However, its non-destructive properties also make MRI a popular method for studying postmortem human brains ex vivo. Compared to in vivo scanning, ex vivo imaging (e.g., of autopsy brains) allows for extremely long MRI experiments that are free of subject motion and other sources of physiological noise, and therefore higher spatial resolution and signal-to-noise ratios than are achievable in vivo. For these reasons, imaging post-mortem human brains with various MRI techniques – e.g., MR Microscopy, Diffusion Tensor Imaging (DTI), High Angular Resolution Diffusion Imaging (HARDI), Diffusion Spectrum Imaging, Magnetization Transfer Imaging (MTI), multi-component T_2-relaxation Myelin Water Imaging (MWI), etc. – has become a popular option (31,32,39,40,65–67,77–81).

There are, however, a few additional challenges in ex vivo MRI that make it more complicated than in vivo imaging. For example, postmortem brains will degrade due to bacteria and autolysis unless chemical fixatives are used for preservation (35). Due to its efficacy and availability, formalin is the most common fixative for tissue preservation (74–76). However, it is known that fixatives alter various MRI properties, as observed in previous studies (64,77,78,82). For example, postmortem interval (PMI) (39,64,83) – i.e., the amount of time between patient death and initiation of tissue fixation – is associated with tissue decomposition (81); and scan interval (SI) (79) – i.e., the amount of time that tissue has been immersed in fixative at the time of MRI scanning – is hypothesized to cause acidity (84), dehydration (83) and protein cross-linking (35,85). It

should be noted that both PMI and SI alter various MRI properties, including: T_2-relaxation, proton density (PD) measurements, fractional anisotropy (FA), apparent diffusion coefficient (ADC), and mean diffusivity (MD). (31,35,36,77,78,82,86–88). However, although these are important topics that should be considered in any postmortem MRI experiments (and likely warrant further investigation in their own right), they are beyond the scope of the current manuscript.

Instead, the intended goal of our protocol is to deal with the other major challenge associated with postmortem, ex vivo MRI scanning – namely, image artifacts that are often caused by magnetic susceptibility interfaces or magnetic susceptibility boundaries. In vivo, the brain is surrounded by cerebrospinal fluid (CSF) and other tissues (including the meninges, skull, and scalp), which create a stable and relatively homogeneous magnetic environment. However, once the brain is removed from this environment, large image artifacts can result from the magnetic susceptibility differences that occur at air-tissue boundaries (89–92). One potential solution to this problem is to scan postmortem brains in situ, before removing them from the skull (93), but this has obvious limitations and is either impractical or impossible in many situations. Another more common approach to mitigating magnetic susceptibility distortions has been to remove the brains and scan them ex vivo in a proton-free fluid called Fomblin (a chemically-inert perfluoropolyether fluorocarbon; Solvay Solexis Inc.), which produces no MRI signal but has a similar magnetic susceptibility to tissue (39,41). However, although this is arguably the "gold-standard" ex vivo imaging approach, there are still several drawbacks. For example, Fomblin is very expensive (> $500 Canadian dollars per liter), and it is not readily available in most pathology labs or MRI centers – making it difficult to obtain (especially in quantities necessary for immersing whole human brains). Furthermore, Fomblin is difficult to completely remove from the surface of the

specimen due to its oil-like properties, and this may interfere with subsequent brain fixation, embedding and/or histological staining.

Therefore, we have developed an alternative approach that involves scanning ex vivo human brains in a MRI-compatible container that is completely filled with either water or formalin solution (i.e., in a magnetic environment similar to in vivo conditions), while taking special precautions to eliminate air bubbles from both the brain and the container. We have found, through trial and error, that the easiest and most effective method to completely eliminate bubbles is to completely immerse the MRI-compatible container in water or formalin, place the brain inside and gently agitate to remove small surface bubbles, and then secure the container lid while completely submerged. In order to document our procedures (and hopefully pass our knowledge on to other researchers) our optimized protocol is described below in detail, and examples of resulting brain images are shown to demonstrate the efficacy of this approach.

2.3 Materials and Equipment

The names and descriptions of all necessary materials are provided in Table 2-1, and optional materials (that are necessary for scanning in formalin) are listed in Table 2-2.

Before working with any new materials, manufacturers' instructions (and material safety data sheets, if applicable) should be carefully reviewed for safe handling, application, disposal, and spill cleanup procedures.

Table 2-1: *Name of necessary materials*

Materials	**Company**	**Comments/Description**
1 gallon (3.8L), wide-mouth, water jug	Coleman	MRI-compatible brain container with interior/exterior dimensions of approximately 5.75/8.00 inches (W) x 5.75/8.25 inches (D) x 9.75/11.75 inches (H). [Available on Amazon or at most camping/outdoor retailers and department stores]
Small bottle or tube of plastic epoxy	Any	To permanently seal the spout and any other openings on the lid of the MRI-compatible brain container. [Available on Amazon or at most hardware stores]
A medium sized, water-tight, rectangular, plastic bucket	Any	Water/formalin overflow bucket. Interior dimensions should be at least as wide, approximately twice as deep, and approximately 9" taller than the brain container (i.e., >8" x ~16" x ~ 22"). [Available on Amazon or at most department stores]
Minimal expansion polyurethane insulating foam	Dow Chemicals Great Stuff ™ Gaps & Cracks Insulating Foam Sealant	To fill the voids between the water/formalin overflow bucket and the MRI-compatible brain container. For full product details, please refer to the Canadian Construction Materials Centre product report (CCMC 13074-L). [Available on Amazon or at most hardware stores and department stores]

5lb barbell weight plate	Any	To keep the MRI-compatible brain container submerged in the overflow bucket during water/formalin filling. [Available on Amazon or at most sporting goods stores and department stores]
Duct tape	Any	To temporarily attach the 5lb weight to the bottom of the MRI-compatible brain container during the water/formalin filling procedure. [Available on Amazon or at most hardware stores]
Extra-large garbage or yard waste bags	Any	To place between the overflow bucket and the MRI-compatible brain container during water/formalin filling. Also to place around the MRI-compatible brain container in the MRI system in case of small drips/leaks from the lid. [Available on Amazon or at most grocery stores and department stores]
Cotton batting	Any	To place inside the top and bottom of the MRI-compatible container (in order to pad the brain specimen). [Available on Amazon or at most sewing/fabric stores and department stores]
Latex or nitrile surgical gloves	Any	To wear while handling brain specimens. [Available on Amazon or at department stores]
Lab coats (or surgical gowns)	Any	To wear while handling brain specimens. [Available on Amazon or from most chemical supply companies]

Multi-Contrast MRI fiducial marker	Any (e.g., Beekley Medical MR-SPOTS Packets™)	To correctly identify right/left hemispheres in subsequent MRI data. [Available upon request in most Radiology Departments and MRI Centers, but can also be purchased from a local medical supply company]
Either stitches or string (and possibly a hemostat or tweezers to tie)	Any	To attach the fiducial marker to remaining dura matter or cerebral vein. [Available in any Pathology Department]
Scissors	Any	To cut duct tape, stitches, yard waste bags, etc. [Available on Amazon, in most department and hardware stores, or in most Pathology Departments]
Human MRI system and head coil (additional flex coil optional)	Any	To acquire whole-brain, ex vivo MRI data. [Need to request access from local Radiology Department or MRI Facility]
Small foam pad or folded sheet	Any	To place between posterior elements of the head coil and the MRI-compatible brain container (in order to hold the container securely in place and reduce vibrations during scanning). [Available in any MRI Facility]

Table 2-2: *Name of Optional Materials (if using Formalin)*

Materials	**Company**	**Comments/Description**
10% phosphate buffered formalin solution	Any	pH-neutral solution for histological tissue (brain) fixation. [Available in most Pathology Departments, but can also be ordered from Sigma-Aldrich (Product ID: HT501128-4L)]
Formaldehyde spill response kits (x2)	Safetec	To safely manage and clean up small formalin spills. [Available from Fisher/Thermo Scientific (Product Name: Safetec Formaldehyde Spill Response Kit; Product ID: 19-314634)]
Fume hood	Any	For safety reasons, formalin solution should only be poured/handled in a well-maintained fume hood. [Available in most Pathology Departments and other "wet lab" spaces]
Face shields	Any	For safety reasons, face shields and other protective clothing should always be worn while pouring/handling formalin solution. [Available in most Pathology Departments, but can also be purchased on Amazon]
Chemical-resistant, shoulder-length gloves	Any	For safety reasons, chemical resistant gloves and other protective clothing should always be worn while pouring/handling formalin solution. [Available in most Pathology Departments, but can also be purchased on Amazon]

Baritainer (for chemical waste disposal)	Any	For discarding excess formalin solution. [Available in most Pathology Departments, but can also be purchased on Amazon]
Formalin neutralizing solution	Any	For neutralizing excess formalin solution. [Available in most Pathology Departments, but can also be purchased through Fisher/Thermo Scientific (Product Name: Formalex™; Product ID: 3120131)]
Heavy-duty (4 mil or 6 mil) polypropylene tubing (12" wide)	Any	For placing around the MRI-compatible brain container before putting it in the MRI system (in case of small drips/leaks from the lid). [Available in most Pathology Departments, but can also be purchased on Amazon]
Industrial heat impulse sealer (at least 12" wide)	Any	For sealing the polypropylene tubing around the MRI-compatible brain container before putting it in the MRI system (in case of small drips/leaks from the lid). [Available in most Pathology Departments, but can also be purchased on Amazon]

2.4 Stepwise Procedures

Please note that all experimental procedures reported herein were carried out with proper consent and prior approval from The University of Manitoba Health Research Ethics Board.

2.4.1 Preparation Steps (to be completed before obtaining an ex vivo brain)

2.4.1.1. Procure a wide-mouth, MRI-compatible plastic container with an air- and water-tight screw-on lid that is large enough to hold a whole human brain, but small enough to fit inside a MRI head coil.[1] We have had excellent results using 1 Gallon (3.8L) Coleman Water Jugs (Model No. 3000000865; Exterior Dimensions: 8" x 8.25" x 12.8"), which: 1) comfortably accommodated full-sized adult human brains, 2) were MRI-compatible, 3) fit inside a standard 12-channel Siemens head coil, and 4) did not produce any noticeable image artifacts.

2.4.1.2. If the lid of the MRI-compatible container has an opening or spout, this should be permanently sealed with plastic epoxy to avoid any accidental leaks or spills in subsequent steps. Please note that proper safety precautions should followed while mixing and handling epoxy (e.g., working in a well-ventilated area and wearing disposable latex/nitrile gloves and safety goggles to avoid contact with your skin or eyes).

2.4.1.3. Obtain a rectangular, water-tight plastic bucket that is at least as wide, approximately twice as deep, and at least 9 inches taller than the brain container described above in section 2.4.1.1. This will give sufficient room for the experimenters to place the smaller container into the larger bucket (and open/close the lid) inside of the larger bucket.

2.4.1.4. *[Note: This step is only necessary for scanning ex vivo brains in formalin during subsequent steps, and is not necessary if scanning in water or saline.]* Wrap the small,

[1] Note that an adult human brain weighs approximately 3.3lbs and has a volume of approximately 1130 cm^3 for women and 1260 cm^3 for men (129).

MRI-compatible brain container described in section 2.4.1.1 (without brain or formalin in it) with a large polyethylene (garbage/yard waste) bag, and place it inside the larger bucket. Then spray one layer (approx. 3-4 inches deep) of expanding polyurethane-based insulating foam sealant into the bottom of the larger bucket (i.e., around the smaller polyethylene-wrapped container) and wait for the polyurethane foam to fully expand and cure (approx. 3-4 hours) before adding another layer. Repeat this process until the expanding polyurethane foam has filled the larger bucket to a depth of 1-2 inches below the top of the smaller polyethylene-wrapped brain container (approx. 3 layers total x 3-4 hours/layer = 9-12 hours). In this way, the brain container serves as its own mold, while the expanding foam insulation fills the voids between the smaller and larger buckets (i.e., to reduce the amount of wasted formalin in subsequent steps). The polyethylene bag is necessary in order to get the brain container out of the larger bucket after the foam dries and hardens. For the expanding polyurethane foam insulation, we used Great Stuff (TM) Gaps & Cracks Insulating Foam Sealant (Dow Chemicals Product Number: 157911). As noted, it is highly recommended that the sealant be applied in layers in order to give ample time to expand and dry between subsequent rounds of application. Also, proper safety precautions should always be used while handling the polyurethane foam insulation (e.g., working in a well-ventilated area and wearing disposable latex/nitrile gloves and safety goggles to avoid contact with your skin or eyes). Then, once the shape is molded and the expanding foam has completely hardened, remove the polyethylene-covered brain container from the larger bucket. The whole objective of this step is to occupy volume inside of the

large bucket so that less formalin will be wasted while filling the smaller bucket in subsequent steps.

2.4.2 Obtaining Whole Postmortem Brain Specimens

2.4.2.1. Before procuring any ex vivo brain samples, it is essential to obtain proper research ethics approval and coordinate with local Neuropathologists to acquire postmortem materials in an ethical and timely fashion.

2.4.2.2. Discuss all study inclusion/exclusion criteria so that the Neuropathologists can screen and select appropriate cases based on clinical history, cause of death, etc.

2.4.2.3. If possible, it is advised that the MRI researcher wait in (or immediately outside of) the autopsy room in order to minimize the interval between brain removal and formalin immersion and/or the initial MRI scan.

2.4.3 Pre-Imaging Steps (to be completed immediately before imaging experiments)

2.4.3.1. Attach a MRI-specific fiducial marker on either the left or right hemisphere (and note the location) to enable proper orientation of the brain during subsequent image acquisition (Figure 2-1A). The fiducial marker can typically be secured with 1-2 stitches around a flap of remaining dura matter (if present) or one of the major superficial cerebral veins.

2.4.3.2. Make sure that the larger bucket from steps 2.4.1.3 and 2.4.1.4 above – i.e., without or with the expanding foam insulation molding, depending on whether the

subsequent preparation will be performed using water or formalin – is available for subsequent steps (Figure 2-1B).

2.4.3.3. Attach a 5lb barbell weight plate to the bottom of the small, MRI-compatible brain container with duct tape (Figure 2-1C). The diameter should be less than or equal to the diameter of the container. Because the container is made of plastic and tends to float in water/formalin, attaching a weight will keep the container submerged. Then wrap the container (with the weight attached) in a large polythene (garbage or yard waste) bag and place it inside the corresponding mold in the larger bucket.

Figure 2-1: *(A) Brain with a marker in the left hemisphere to detect left-right sides of the brain during image acquisition/ processing; (B) A polyurethane-based insulating foam sealant sprayed inside the custom bucket to place the container and lid; (C) Weight attached under the container to restrain it from floating.*

2.4.3.4. Cut two pieces of thick cotton and place one of them inside the bottom of the brain container to create a protective layer that is approximately 1-1.5 inches thick (Figure

2-2A). The second piece of cotton will be used later to protect the brain from the lid (and will be added in step 2.4.3.11, before the lid of the container is secured).

2.4.3.5. Slowly pour water or formalin into the small, MRI-compatible brain container, and continue filling until the water/formalin level overflows into the larger container and is approximately 1 inch above the top of the smaller container. NOTE: For this study, 10% phosphate buffered formalin solution was used, which is widely available for routine histopathology (94). CAUTION: Proper safety precautions should always be strictly adhered to while handling/pouring formalin (e.g., working in a fume hood while wearing closed-toe shoes, long pants, a lab coat or surgical gown, a face shield, and shoulder-length, chemical-resistant gloves), and a formaldehyde spill response kit (e.g., Fisher Scientific Product Number: 19-314634) should be readily accessible.

2.4.3.6. Squeeze the cotton at the bottom of the MRI-compatible container under the water/formalin for approximately 1 minute to get rid of any air bubbles, and then splay it out in the bottom of the container. A freshly extracted brain is jelly-like and can be easily deformed, so using cotton at the bottom of the container minimizes the risk of tissue damage.

2.4.3.7. Very gently, place the brain inside of the small, MRI-compatible brain container (i.e., carefully with both hands). In our experience, the orientation of the brain in the container does not matter, so either the anterior or posterior portion of the brain can be oriented toward the lid. Nonetheless, we recommend being consistent across subjects and/or time-points within a study. NOTE: In order to reduce the chances of having large air bubbles trapped in the lateral ventricles, water or formalin can be injected with a syringe directly into the ventricles (e.g., through the occipital lobe) to

displace trapped air. However, it is highly recommended to perform this step only after consultation with the collaborating Neuropathologist (i.e., to avoid compromising or interfering with subsequent clinical examinations, etc.).

2.4.3.8. Continue pouring water or formalin until the level is at least a few inches (i.e., greater than the depth of the lid of the MRI-compatible brain container) above the opening of the brain container (Figure 2-2B). NOTE: Especially if using formalin, the experimenter should use his/her judgment to estimate the minimum amount of overflow necessary to complete the remaining steps and seal the container beneath the fluid level. This will minimize formalin waste, and more can always be added later if necessary.

2.4.3.9. The brain should then be slowly and gently agitated by hand (e.g., rotated left/right on its anterior/posterior axis) – while constantly submerged within the MRI-compatible container – for 2-3 minutes in order to ensure that no air bubbles are trapped along the cortical surface or under the cerebellum. The experimenter should use their judgment to agitate the sample enough to remove any visible bubbles, while ensuring that the brain specimen is not damaged in the process.

2.4.3.10. The second piece of cotton should then be submerged in the water or formalin, squeezed for approximately 1 minute to remove any air bubbles, and then splayed out (while constantly submerged) over the brain at the top of the MRI-compatible container.

2.4.3.11. The lid of the MRI-compatible container should then be completely submerged and manipulated (if it hasn't been already) to remove any bubbles before closing it tightly beneath the level of the water or formalin (Figure 2-2C). Make sure that no cotton is

stuck in the threads, and that the lid is not cross-thread before tightening. NOTE: Screwing the lid on tightly is essential to prevent leaks in later steps; however, over-tightening may strip or distort the threads, so do not apply too much force.

Figure 2-2: *(A) Container and lid placed in the large bucket with a polythene bag wrapped around with some cotton in the bottom; (B) Brain inside the bucket with formalin flowing over; (C) The container with closed lid under the formalin*

2.4.3.12. After ensuring that the lid is secure, slowly and gently pull the MRI-compatible container out of the water or formalin in the larger bucket (i.e., using the handle if possible). Then detach the duct tape and the weight from the bottom and use paper and/or cotton towel to completely dry the exterior of the container before examining for any potential leaks (around the lid, or otherwise). NOTE: If leaks are identified, check to ensure that the lid is tight (but not over-tight), and if leaks persist, re-

submerge the entire container, remove the lid and try again (ensuring that no cotton gets caught between the threads).

2.4.3.13. Especially if formalin was used to fill the brain container, it is recommended to heat-seal the entire MRI-compatible container inside of a heavy-duty (4 mil or 6 mil) polypropylene bag or tubing to catch any potential drips or minor leaks (and to act as a safeguard in the unlikely event that the container is dropped or damaged during transport). Make sure to squeeze the bag before sealing to reduce the amount of air trapped inside the bag as much as possible. If too much air is in the bag, it may not fit in the MRI head coil in later steps. NOTE: Carefully check the sealed bag and, if in doubt, either repeat the previous step or add another layer of heat-sealed polypropylene tubing.

2.4.3.14. Finally, the brain container (whether heat-sealed in polypropylene bags/tubing or not) should be placed in 2 layers of large polyethylene (garbage/yard waste) bags – with the ends tied securely – to add an additional safeguard from potential drips or leaks during transport and/or MRI scanning. Again, make sure to squeeze as much air out of the bags as possible before tying (so that everything will fit inside of the MRI head coil).

2.4.3.15. Following step 2.4.3.14 above, the brain specimen is ready to be transported to the MRI facility, placed in the head coil, and scanned using the desired MRI pulse sequences.

2.4.3.16. The water or formalin waste (still in the larger bucket following step 2.4.3.13 above) can either be saved for later or properly disposed of. NOTE: Water can likely be poured down any sink or autopsy table in the Pathology Department (check with a

Pathologist or Pathology Technologist), but formalin will need to be disposed of more carefully (see step 2.4.3.17-2.4.3.19 below).

2.4.3.17. If formalin was used, it should be poured slowly and carefully (using a funnel) out of the polyethylene bag (in the large bucket) into a chemical Baritainer that has been specifically marked for formalin waste. Once there is very little formalin left in the polyethylene bag, carefully remove it from the large container and cut one of the bottom corners with scissors to drain any remaining formalin into the Baritainer. Then add the proper amount of formalin-neutralizing compound to the Baritainer and wait the specified amount of time before discarding the neutralized formalin. NOTE: The duct tape, polyethylene bags, and any paper towels, etc. with formalin on them should be placed into a garbage bag (which should then be securely tied) before removing from the fume hood and placing into an appropriate disposal bin (check with a Pathologist or Pathology Technologist).

2.4.3.18. Leave the large bucket, 5lb weight and shoulder-length, chemical-resistant gloves in the fume hood until the formalin has completely evaporated.

2.4.3.19. Finally, remove latex/nitrile gloves, safety glasses or face shield, and lab coat or surgical gown, and wash hands thoroughly.

2.4.4 Recommended Set-Up for MRI Scanning

2.4.4.1. If using a two-part head coil for scanning, install the posterior elements of the head coil.

2.4.4.2. Out of an abundance of caution, we recommend taping a large polyethylene sheet or bag over top of the posterior head coil elements and patient table in case of small drips or leaks. NOTE: Although the possibility of a leak or spill is extremely unlikely if all of the aforementioned procedures are strictly adhered to, in case of emergency, a second formaldehyde spill response kit should be purchased and stored at the MRI facility if formalin is being used.

2.4.4.3. Place the MRI-compatible brain container (sealed in multiple layers of plastic bags) with the handle/lid-side facing outward on a folded sheet or cylindrical foam pad to reduce vibrations and keep the container in position during the MRI scanning session.

2.4.4.4. Install the anterior elements of the head coil around the MRI-compatible brain container (Figure 2-3). NOTE: If possible (i.e., if the MRI facility has a large flex coil and the system has enough receiver channels to accommodate it in addition to the head coil), we have found that it is also beneficial to strap, tape, and/or brace a large 4-channel (knee) flex coil over any potions of the brain container extending beyond the inferior portion of the head coil (i.e., since the lid and handle extend slightly beyond our 12-channel Siemens head coil).

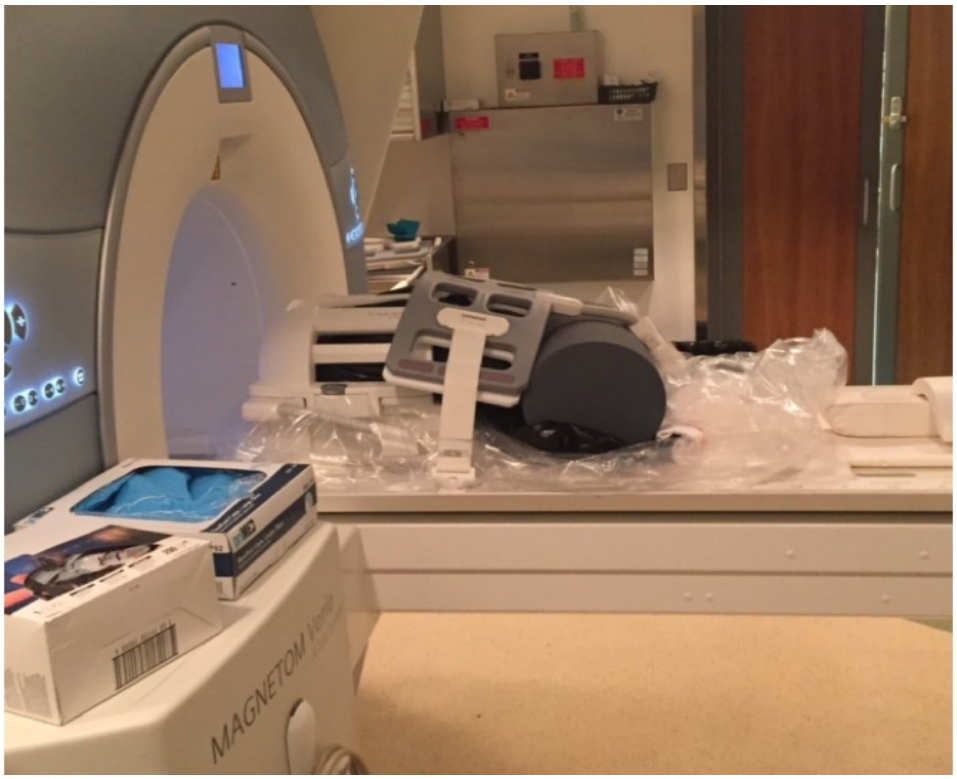

Figure 2-3: *Setup at the MRI facility with a 12-channel head coil and a 4-channel (knee) flex coil. Cylindrical foam padding was placed under the MRI-compatible container to add stability and minimize vibrations during MRI scanning.*

2.4.4.5. Acquire a series of localizer scans to: 1) check for severe artifacts arising from bubbles in the brain and/or MRI-compatible container, 2) properly orient the brain, and 3) assign slice positions for subsequent data acquisition.

2.4.4.6. Acquire high-resolution, whole-brain, ex vivo MRI data (hopefully without magnetic susceptibility artifacts from air bubbles).

2.4.5 Removing the Brain from the MRI-Compatible Container and/or Changing Formalin

NOTE: If scanning a brain that has not already been completely fixed, the specimen will either need to be removed from the MRI-compatible container (and placed back in a large formalin fixation bucket) or the formalin in the MRI-compatible container will need to be changed every few days (due to the limited volume of formalin within the container). If this is the case, it is recommended that the following steps be performed.

2.4.5.1. Bring the container from the MRI center back to the formalin changing facility and put on proper safety equipment (see above in step 2.4.3.4).

2.4.5.2. In the fume hood, remove the polyethylene and polypropylene bags surrounding the MRI-compatible brain container with sharp scissors.

2.4.5.3. Following the procedures outlined in step 2.4.3.2, attach a 5lb weight to the bottom of the MRI-compatible brain container, place it in a large polyethylene bag, and then gently insert it into the corresponding mold in the large bucket.

2.4.5.4. Slowly unscrew the lid of the container and remove the cotton from the top of the container.

2.4.5.5. If removing the brain for long-term storage or follow-up histopathology, very gently lift it (with two hands) into a larger, long-term storage bucket that has been filled with fresh formalin and dispose of the used formalin according to steps 2.4.3.16-2.4.3.18 above.

2.4.5.6. If changing the formalin and keeping the brain in the MRI-compatible container, please follow steps 2.4.5.7-2.4.5.9 below.

2.4.5.7. Carefully pour the used formalin (using a funnel) into a chemical Baritainer that has been specifically marked for formalin waste. NOTE: If two people are involved, this can be done without removing the brain from the MRI-compatible container (i.e., while one person pours the formalin, the other one gently holds the brain from sliding out of the container). However, if working alone the brain should be temporarily removed from the MRI-compatible container and placed into a separate bucket of formalin.

2.4.5.8. Once all of the used formalin has been removed, new formalin can be poured into the MRI-compatible brain container following the procedures outlined in steps 2.4.3.4-2.4.3.19.

2.4.5.9. Then, add the proper amount of formalin-neutralizing compound to the Baritainer, and wait the specified amount of time before discarding the neutralized formalin, according to steps 2.4.3.16-2.4.3.19 above.

2.5 Anticipated Results

In order to illustrate the image quality that can be obtained following the aforementioned protocol, two whole human brains were scanned at room temperature (approx. 22°C) using a whole-body 3T Siemens Magnetom Verio scanner (Siemens Healthcare, Erlangen, Germany), equipped with a standard 12-channel head coil and a large 4-channel (knee) flex coil to ensure adequate/uniform signal across the entire field of view (FOV) of the MRI-compatible brain container (Figure 2-3). For the first brain, the optional procedure in step 3.3.8 was performed (i.e., to inject the ventricles with formalin), while this option was skipped for the second brain sample (i.e., to show the types of artifacts that can result from air trapped within the ventricles) (Figure 2-4).

MRI data were acquired from each brain after approximately 168 hours of formalin fixation, and were scanned in a formalin-filled container. Representative data were acquired using three different pulse sequences (Figure 2-4), including: 1) a spin-echo EPI diffusion tensor imaging (DTI) sequence (95) with isotropically-distributed diffusion-weighting along 30 directions (b = 700s/mm^2, plus five b = 0 s/mm^2 images), TR = 8800ms, TE = 73.6ms, flip angle = 180 degrees, number of slices = 55, field of view = 240mm x 240mm, spatial resolution = 1.25mm x 1.25mm x 2.5mm, number of averages = 2, acquisition time = 10.27 minutes; 2) a 3D T_1-weighted magnetization prepared rapid gradient echo (MPRAGE) (91) with TR = 1900ms, TE = 2.49ms, TI = 900ms, flip angle = 9 degrees, field of view = 250mm x 250mm x 176mm, spatial resolution = 0.49 x .49 x 0.98 mm, number of averages = 1, acquisition time = 4.40 minutes; and 3) a 3D MP2RAGE, which is a self bias-field corrected sequence for improved segmentation and T_1-mapping at high field (96) with TR = 5000ms, TE = 2.87ms, TI_1 = 700ms, TI_2 = 2500ms, flip angle = 5 degrees, FOV = 234mm x 256mm x 176mm, spatial resolution = 1.82mm x 1.82mm x 1.00mm, number of averages = 1, and acquisition time = 5.28 minutes.

Overall, the results obtained after using this technique were excellent – especially after injecting the ventricles with formalin. A sample of each image type is shown below in Figure 2-4, where it can be seen that even in the DTI data – which are generally sensitive to even small magnetic susceptibility distortions (97)– the images appear sharp and artifact-free. However, the bottom row of the figure shows what can happen if air gets trapped in the lateral ventricles and the optional water/formalin injection is not performed in step 2.4.3.8.

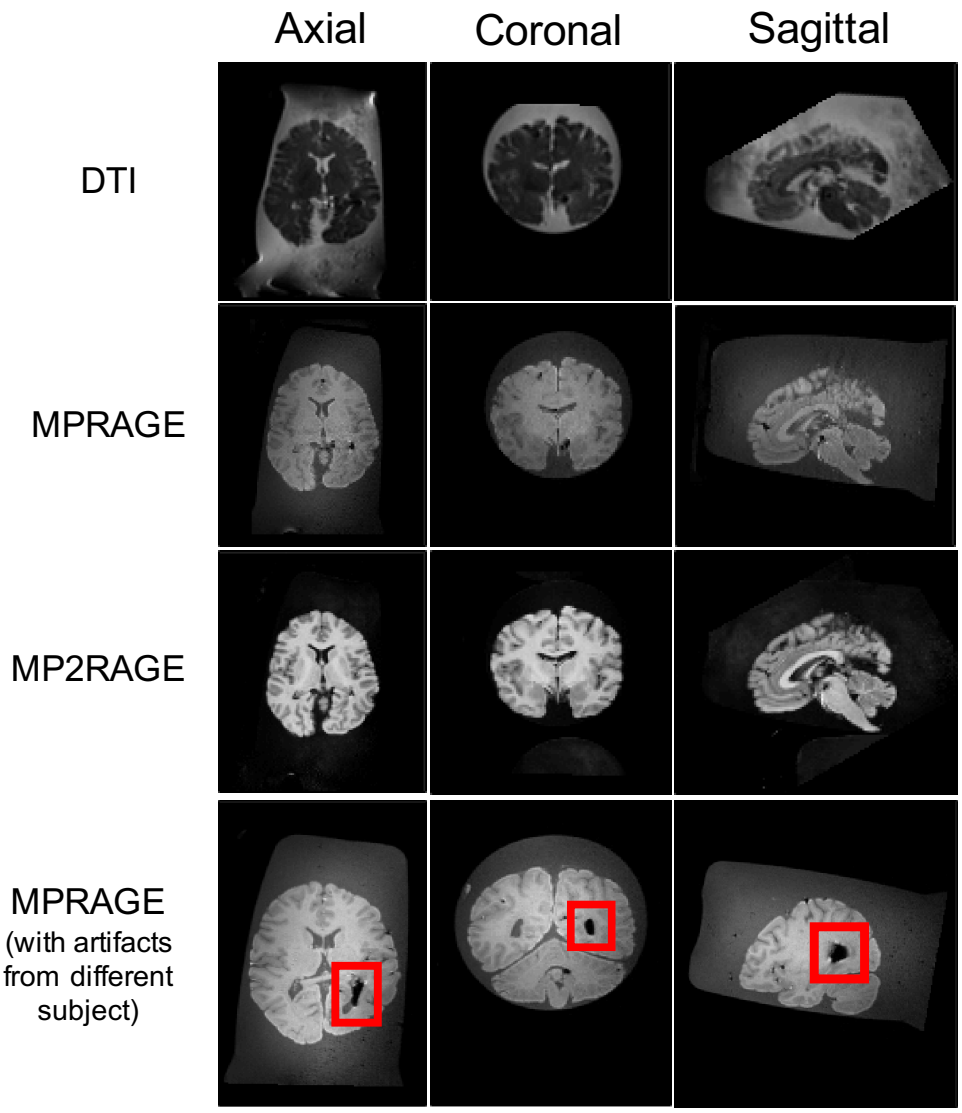

Figure 2-4: *Axial, coronal and sagittal slice views of a 71-year old female brain acquired using the aforementioned MRI sequences following the protocols of this report. The image artifact (shown in red box) was caused by air bubbles inside the ventricle.*

2.6 Discussion

Although there are many potential sample preparations for ex vivo MRI of human brain tissue, more ex vivo studies have been done on fixed brain slices, tissue sections, or hemispheres than on whole human brains. However, there are several obvious advantages to scanning whole brains, especially for exploratory imaging (e.g., to guide subsequent pathological examinations), examining diffuse pathologies, or for things such as whole brain volumetric analyses. Therefore, the purpose of this paper was to introduce an easy and affordable protocol for conducting ex vivo MRI experiments on whole human brains.

This protocol addresses many of the limitations reported in previous ex vivo imaging studies, including: air cavities/bubbles, motion sensitivity, high cost, and the potential need to regularly change fixative solution. Air bubbles, in particular, are a common and significant problem for ex vivo image acquisition if not removed properly. Hence, the initial localizer MRI images should be checked, and if air bubbles are observed inside the ventricles or along the cortical surface, the scan should be stopped until the problem can be resolved (since information in those regions will be compromised in subsequent scans as well).

Motion is another problem that needs to be properly addressed. Previous studies have embedded brains or brain tissue in agarose gel – either in a rectangular container (82), plexiglass cradle (89), or cardboard frame (78) – to ensure stability while scanning. While this approach is likely very effective for controlling bulk motion, it does not isolate table vibrations that are quite prominent during certain types of scanning (e.g., diffusion imaging); plus, embedding in agarose prior to scanning may not be possible (e.g., depending on when in the fixation process scanning needs to

occur, what follow-up procedures clinical Pathologists need to perform after scanning, etc.). However, although we suggest using cotton bats at the top and bottom of the brain (inside the MRI-compatible container) and a foam pad (outside the container) in an attempt to resist different kinds of motion during the scans – not to mention the fluid barrier inside the container – these measures may not completely eliminate bulk motion or scanner-related vibrations either. Therefore, we still recommend that proper care be taken during subsequent image processing (e.g., applying motion-correction algorithms, etc.).

Although the proposed ex vivo scanning preparation has several advantages (discussed above), the 1 gallon (3.8L) container presents a couple of potential limitations. First, this preparation has been optimized for human MRI systems and the container will not fit in most small-bore 7T, 9.4T, or 11.7T preclinical imaging systems. Second, we have shown that the container fits very well within the standard 12-channel Siemens head coil, but coils with different configurations (e.g., Siemens 32-channel and 64-channel coils) and coils from other manufacturers/vendors (e.g., Philips, GE, etc.) may not accommodate the container. Therefore, before using this setup with other coils, the container should be tested ahead of time to ensure that it will physically fit. If it does, then it should be centered as much as possible between the anterior and posterior elements of the coil to produce the most uniform SNR profile throughout the brain; otherwise (if it will not fit), surface coils could be used as an alternative. However, if surface coils are being considered, it is perhaps worth noting that reducing the distance between the coil and the brain sample (e.g., using a smaller, more conformal, and/or thinner-walled sample container) would improve the SNR of the resulting images, all else being equal.

Finally, it should be emphasized that the polyurethane-based insulating foam, plastic epoxy, and formalin are toxic, and that the brain specimens themselves are a significant biohazard risk. Proper care should therefore be taken when working with these materials. As a rule, we would recommend that anyone planning to replicate our procedure should: 1) read the material safety data sheets (MSDS), and 2) carefully review all of the manufacturer's instructions before handling these or any other chemicals they plan to work with. Moreover, we would recommend that at least two people are present at all times during these procedures.

In conclusion, ex vivo human brain MRI can provide useful information on both the macroscopic/anatomical and microscopic/microstructural level; however, proper sample preparation is an important component for achieving good image quality. Although the quality of ex vivo MRI data also depends on other factors (i.e. scanner hardware, image acquisition parameters, image pre- and post-processing, etc.), none of these matter if the images are degraded by magnetic susceptibility artifacts. Therefore, the steps described in this report should help both clinicians and researchers easily and economically acquire high-quality, artifact-free ex vivo MR images of whole postmortem human brain samples.

2.7 Author Contributions

CRF designed the protocol with contributions from KMM. ASS, CRF, and KMM performed the experiments. ASS analyzed the results. ASS wrote the manuscript with contributions from CRF and KMM.

2.8 Funding

This work was funded by The University of Manitoba (UofM), The Natural Sciences and Engineering Research Council of Canada (NSERC), The Winnipeg Health Sciences Centre Foundation (HSCF), and Brain Canada.

2.9 Conflict of Interest Statement

The authors have no conflicts of interest to disclose.

2.10 Acknowledgements

The authors acknowledge funding from The University of Manitoba (UofM), The Natural Sciences and Engineering Research Council of Canada (NSERC), The Winnipeg Health Sciences Centre Foundation (HSCF), and Brain Canada. The authors would also like to thank Teresa Figley and all of the wonderful MRI Technologists at the Winnipeg Health Sciences Centre (particularly Paul Barrette, Brandi Adolphe, Laura Garry, Cynthia Kulczycki, Mike Gordillo, Cindy Storey, Alexi Thiessen, and Caitlin Gallant) for helping with the MRI scheduling and data acquisition, and to all of the Pathology Technicians (particularly Samuel Findlay, Cheryl Fernando, Terry Beach, Chris Kacsmar and Marvin Mayuga) for their assistance in procuring and preserving the brain specimens.

Chapter 3 : Quantitative ex vivo MRI changes due to progressive formalin fixation in whole human brain specimens: Longitudinal characterization of diffusion, relaxometry, and myelin water fraction measurements at 3T

3.1 Abstract:

Purpose: Postmortem MRI can be used to reveal important pathologies and establish radiology-pathology correlations. However, quantitative MRI values are altered by tissue fixation. Therefore, the purpose of this study was to investigate time-dependent effects of formalin fixation on MR relaxometry (T_1 and T_2), diffusion tensor (fractional anisotropy, FA; and mean diffusivity, MD), and myelin water fraction (MWF) measurements throughout intact human brain specimens.

Methods: Two whole neurologically-healthy human brains were immersed in 10% formalin solution, and then scanned at 13 time-points between 0 and 1032 hours. Whole brain maps of longitudinal (T_1) and transverse (T_2) relaxation times, FA, MD, and MWF were generated at each time-point to illustrate the changes over time, and region-of-interest analyses were performed in eight brain structures to quantify the changes with progressive fixation.

Results: Although neither of the diffusion measures (FA nor MD) showed significant changes as a function of formalin fixation, both T_1 and T_2-relaxation times were significantly decreased, and MWF estimates were significantly increased.

Conclusions: These results suggest that T_1-relaxation, T_2-relaxation and myelin water fraction estimates must be performed very early, or at consistent time-points, in the fixation process to avoid formalin-induced changes compared to in vivo values or between samples, respectively.

3.2 Introduction:

Postmortem MRI has become a popular tool for assessing brain microstructure, structural development, and pathology with high resolution, and it has been increasingly used in combination with histological staining and proteomic approaches to probe underlying mechanisms of various quantitative imaging methods (67,98–101). From a biomedical imaging perspective, ex vivo MRI of postmortem tissue offers several benefits over in vivo scanning, including no participant or physiological (cardiac, respiratory, pulsatile etc.) motion artifacts and no time restriction for data acquisition, which in turn, allows images to be acquired with much higher spatial resolution and signal to noise ratio (SNR) (39,65,79). As a result, ex vivo MRI offers unprecedented potential to discover novel and interesting features of postmortem tissue architecture both in neurologically healthy and diseased brains by applying advanced MRI techniques such as, diffusion tensor imaging (DTI) (102), relaxometry methods (T_1, T_2 and T_2^*) (103–106), multi-component T_2-relaxation myelin water imaging (MWI) (107) etc. For example, a few ex vivo studies have effectively used MWI with histopathology, and validated a unique MR property- myelin water fraction (MWF) as a marker of myelin integrity using tissue samples that were affected by Multiple

Sclerosis (MS) (52,53,62,63). Thus, such modern techniques offer valuable quantitative measures for research applications and can identify microstructural pathologies or inconsistencies in postmortem brains that may have remained unnoticed during macroscopic inspection in routine autopsies.

However, to prevent postmortem degradation, tissues are typically fixed with chemical solutions – most commonly phosphate buffered formalin (aka, formaldehyde or methanal) (74–76) – that are known to alter various MRI properties. For example, formalin fixation is known to shorten the T_1- and T_2-relaxation times of tissues compared to their in vivo state after a certain period (77–79,108). While the exact reasons of formalin-induced effects are still debatable, a few postmortem studies on non-human brains and small human brain tissue samples have rationalized these effects as a function of temperature (42,109,110), postmortem interval (i.e., the time elapsed between death and the start of fixation) (39,64,83), scan interval (i.e., the tissue fixation time) (79), MR parameters (82), or embedding media (111).

In order to better address the concerns related to postmortem human brains, it is extremely important to characterize the changes of different MR properties in non-diseased human brains due to formalin fixation using state-of-the-art MRI techniques. Thus, in this work, we demonstrated the quantitative changes of DTI-based fractional anisotropy (FA) and mean diffusivity (MD), relaxation times (T_1, T_2) and T_2-relaxation based MWF measurements in a number of deep gray and white matter structures to explain the possible implications of progressive formalin fixation in a whole human brain. To the best of our knowledge, no prior studies have comprehensively characterized the MWF changes along with other MR-based properties in

formalin-fixed brains, and ours is the first reported work of its kind. This investigation is expected to offer a baseline for future ex vivo studies on postmortem brains, which may help us to further comprehend the underlying pathology of neurologically diseased brains.

3.3 Methods:

3.3.1 Sample Preparation

This study was conducted with prior approval from the University of Manitoba Biomedical Research Ethics Board (BREB). Two human brain specimens – both female (Subject 1 = 71 years old; Subject 2 = 74 years old) – were obtained with prior consent. Each patient's medical history was pre-screened by a neuropathologist to exclude cases with neurological disorders, medico-legal cases (i.e., those with unknown or unnatural cause of death) and pediatric cases. Both brains were subjected to a standard neuropathology examination following the study to ensure that incidental pathological findings were not identified. Each brain was carefully extracted as soon as possible after death (Subject 1 = 33 hours; Subject 2 = 55 hours), remaining dura matter was carefully removed, an MRI fiducial marker was attached to facilitate the orientation of cerebral hemispheres in the acquired images, and the whole brain was immersed in 10% phosphate buffered formalin (PBF) solution inside an air- and liquid-tight MRI-compatible container following a previously-reported ex vivo MRI protocol (1). For Subject 1, formalin was carefully injected into the posterior horn of the lateral ventricle using a needle syringe to eliminate a large air bubble that was identified during the initial scan, but this was not necessary for Subject 2 (as no trapped air bubbles were observed). Following the standard neuropathology procedures at our site, formalin was replaced approximately once per week. Table 3-1 shows the times of formalin change for each subject.

Table 3-1: *Time of formalin change in hours after first immersion in the container*

Formalin Change	Subject 1 (hours)	Subject 2 (hours)
1st	120	24
2nd	288	168
3rd	500	336
4th	672	500
5th	-	672

3.3.2 Image Acquisition

Each brain specimen was scanned at room temperature (22°C ± 1°C) at the same 13 time points (i.e., 0, 12, 24, 46, 120, 168, 211, 288, 336, 500, 672, 840 and 1032 hours) after the initiation of formalin fixation. All MRI scans were performed in a whole-body 3T Siemens Magnetom Verio scanner (Siemens Healthcare, Erlangen, Germany), equipped with 12-channel head coil and a large, 4-channel (knee) flex coil to acquire uniform signal throughout the field of view (FOV) (1), and foam pads were used to hold the container in place and reduce scanner vibrations (1). The total scan time for each MRI session was approximately 60 minutes. Diffusion measurements were performed by means of a single-shot fast 2D segmented spin echo, echo planar imaging (SE-EPI) sequence, that had the following scan parameters: 30 diffusion-encoded images (b = 700 s/mm^2), 5 reference images (b = 0 s/mm^2), Repetition Time (TR) = 8800 ms, Echo Time (TE) = 73.6 ms, Flip Angle = 180°, Number of Slices = 55, Slice Thickness = 2.5 mm, Matrix Size = 192 x 192, FOV = 240 x 240 mm^2, Resolution = 1.25 x 1.25 x 2.5 mm^3, Number of Averages = 2, Total Scan Time = 11 min. T_1-relaxometry data were acquired using a 3D magnetization prepared rapid acquisition gradient echo sequence with two inversion times (MP2RAGE) (96), and the T_1-

weighted images with the longer inversion time were also used for subsequent image processing steps, including co-registration and spatial normalization. The parameters for this sequence were: TR = 5000 ms, TE = 2.87 ms, Inversion Time (TI) = 700 ms and 2500 ms, Flip Angle = 4° and 5°, Matrix Size = 128 x 140 x 176, FOV = 256 x 234 x 176 mm^3, Resolution = 1.83 x 1.83 x 1 mm^3, and Acquisition Time = 11 min. However, due to a temporary software license issue for the MP2RAGE sequence, conventional T_1-weighted images were obtained using a 3D magnetization prepared rapid acquisition gradient echo (MPRAGE) sequence (112) in order to facilitate co-registration, spatial normalization and image segmentation for the first four time points (i.e., 0, 12, 24 and 46 hour scans) of Subject 1. The parameters for this sequence were: TR = 1900 ms, TE = 2.49 ms, TI = 900 ms, Flip Angle = 9°, Matrix Size = 512 x 512 x 176, Resolution = 0.49 x 0.49 x 0.98 mm^3, FOV = 250 x 250 x 172 mm^3, and Scan Time = 5 min. A multi-echo 3D combined Gradient and Spin Echo (GRASE) sequence was used to acquire images with 32 different echo times (113), and was used for subsequent T_2-relaxometry and multi-component myelin water imaging measurements (50). Scan parameters were: TR = 1030 ms, First TE (TE1) = 10 ms, Echo Train Length (ETL) = 32, Echo Spacing (ESP) = 10 ms, Flip Angles = 90° (excitation) and 180° (refocusing), Matrix Size = 160 x 120 x 22, FOV = 240 x 180 x 110 mm^3, Resolution = 1.25 x 1.25 x 5 mm^3, Acquisition Time = 15 min.

3.3.3 Image Processing

All images were preprocessed with a customized pipeline, using a combination of software tools, including: 1) The FMRIB software library (FSL) *[Oxford Centre for Functional MRI of the Brain, Oxford, UK]*, 2) Medical Image Processing, Analysis, and Visualization (MIPAV) *[Centre for Information Technology, NIH, Bethesda, MD, USA]*, 3) MATLAB *[The MathWorks Inc., Natick,*

MA, USA], 4) Statistical Parametric Mapping (SPM12) *[Wellcome Trust Centre for Neuroimaging, London, UK]*, and 5) MRIStudio *[Johns Hopkins University, Baltimore, MD, USA]*.

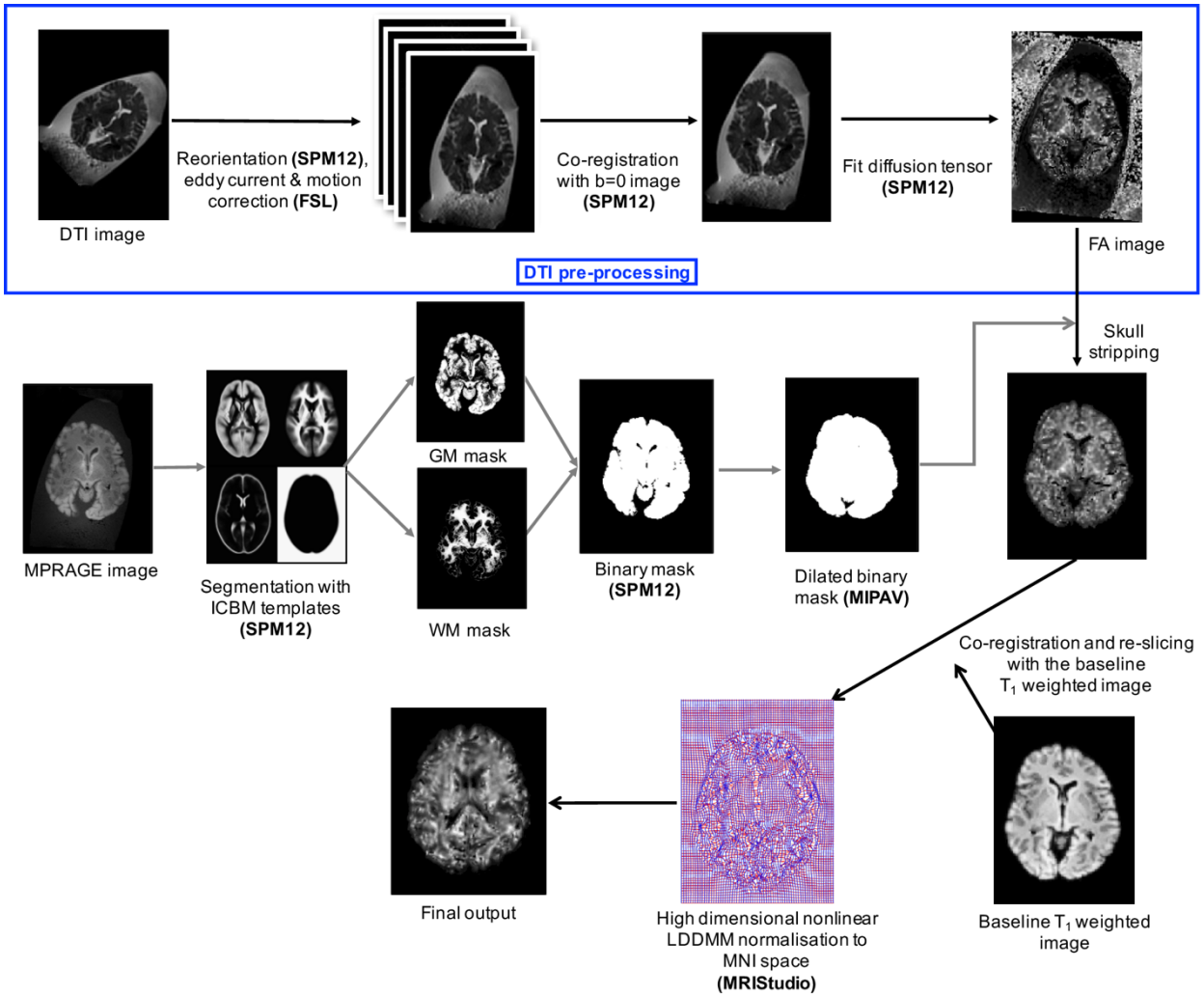

Figure 3-1: *Multistage image processing pipeline for ex vivo postmortem brain MR imaging.*

Figure 3-1 shows the total image preprocessing pipeline. Briefly, the raw DICOM images from the scanner were converted to NIFTI format and manually reoriented to the anterior commissure - posterior commissure (AC-PC) plane using SPM12 to facilitate subsequent automated co-registration across time points and image modalities. To get rid of unnecessary appearance of the

container and formalin in the images, we used the 'old segmentation' (114) tool in SPM12 and created a binary mask of the grey and white matter segments from the T_1-weighted images. These binary masks were dilated in MIPAV using a 5x5x5-24 connected kernel before they were used for skull-stripping. All axial DTI images were eddy current corrected and motion corrected before going through the fit diffusion tensor (FDT) tool (115,116) of SPM12 which generated FA and MD maps. T1-relaxation maps were automatically calculated on the MRI scanner console – through the Siemens Image Reconstruction Environment (IRE) – using the MP2RAGE sequence (46). T_2-relaxation maps were calculated offline from multi-component multi-echo T_2-relaxation data on a voxel-by-voxel basis using stimulated echo compensation (i.e., by taking the signal contribution from stimulated and indirect echoes arising from imperfect radiofrequency (RF) refocusing pulses) (104,117). This method was based on the extended phase graph algorithm (118), and the RF pulse shapes and sequence timing were used to fit complete spin response. The MWF maps were calculated from the 3D GRASE sequence using multi-exponential T_2 fitting for different water compartments while compensating for stimulated and indirect echoes due to imperfect refocusing pulses (55,107,118). The MWF within each voxel was obtained from the geometric mean of the T_2 distribution from myelin water (~10-40 ms) divided by the geometric mean of the T_2 distribution due to intra- and extra-cellular water (~100-200 ms) plus the myelin water (~10-40 ms), as previously described (50).

In order to spatially normalize the data from both subjects, all time-points, and all contrasts, the T_1- weighted data of the first four time points from each subject were spatially normalized in MRIStudio to the Johns Hopkins University (JHU) T_1 brain template in Montreal Neurological Institute (MNI) space (119). This was accomplished using a two-stage warping procedure

consisting of a 12-parameter affine (linear) transformation, followed by high-dimensional, non-linear normalization with the large deformation diffeomorphic metric mapping (LDDMM) algorithm (120) with cascading alpha values of 0.01, 0.05 and 0.002 (121). Later, the respective combined transformation matrices (i.e. linear affine and non-linear LDDMM) were applied to the T_1-weighted image and the rest of the co-registered images (i.e., FA, MD, T_1, T_2 and MWF maps) from each time-point. Since the T_1-weighted image contrast was reduced and the shape of the brain was presumed to be constant (due to the fixation beyond 120 hours) during time points 5 to 13, the normalization parameters from time point 4 were applied to subsequent time points after co-registering the native-space images in SPM12.

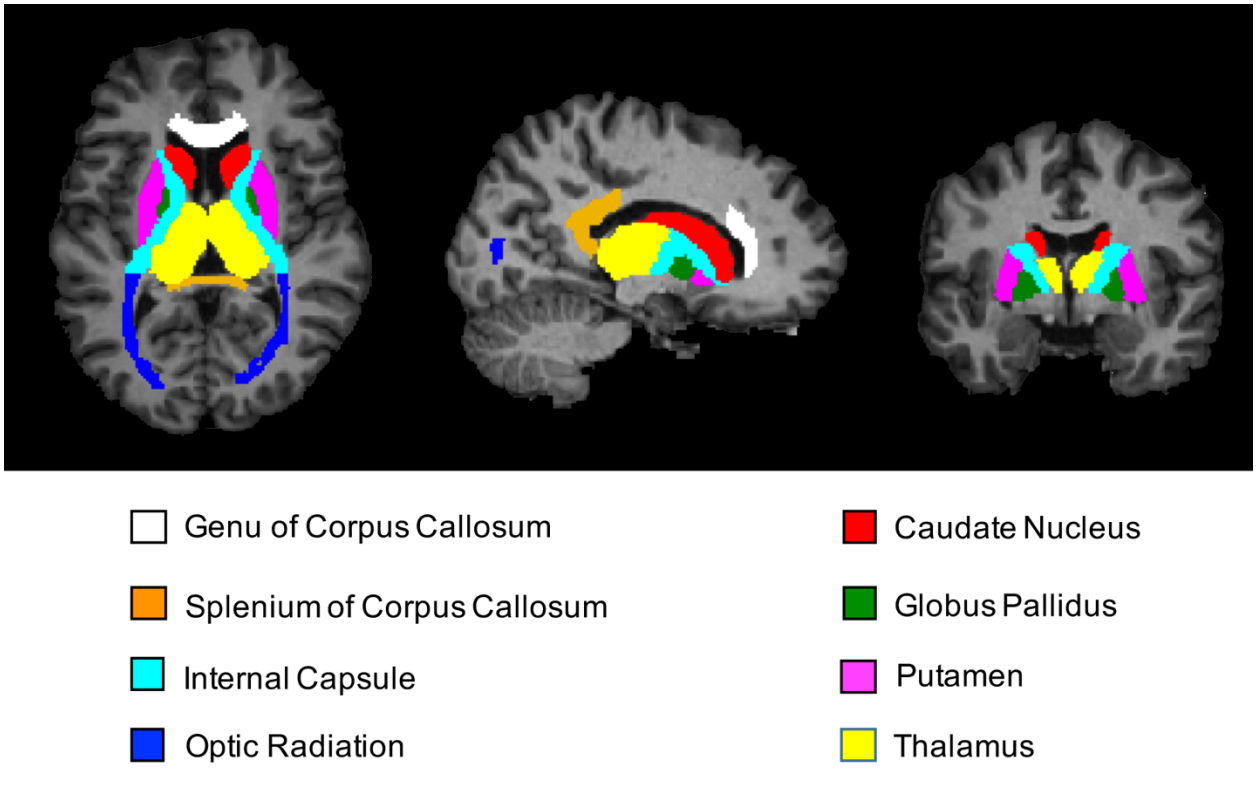

Figure 3-2: *T_1-weighted MPRAGE images (axial, sagittal, and coronal view) showing regions of interest (ROIs) extracted from JHU_MNI_SS atlas. Colored ROIs indicates 4 deep white matter (Genu of Corpus Callosum, Splenium of Corpus Callosum, Internal Capsule and Optic Radiation) and 4 deep grey matter (Caudate Nucleus, Putamen, Globus Pallidus and Thalamus) structures.*

After all of the images were normalized, SPM12 was then used to map the spatiotemporal changes due to formalin fixation – on a voxel-wise level throughout the entire brain – by subtracting the baseline FA, MD, T_1 relaxometry, T_2 relaxometry, and MWF maps from each of the subsequent time points. Region of interest (ROI) analyses were performed using ROIEditor and 3D ROIs chosen from the JHU_MNI_SS ("Eve") atlas in four deep WM and four subcortical GM structures, including: the Genu of the Corpus Callosum (GCC), Splenium of the Corpus Callosum (SCC), Optic Radiation (OR), Internal Capsule (IC), Putamen (Put), Thalamus (TH), Globus Pallidus (GP), and Caudate Nucleus (CN). Figure 3-2 shows the position of these ROIs in axial, sagittal, and coronal views. For bilateral ROIs, corresponding FA, MD, T_1, T_2 and MWF values for each subject were averaged across hemispheres.

3.3.4 Statistical Analyses

All data were analyzed using SPSS 23.0 *[International Business Machines Corporation (IBM), Armonk, NY, USA]*. Spearman rank-correlation coefficient (r_s) was used to assess correlations between MRI measures and fixation time. Two-tailed tests were performed, and only ROIs showing Bonferroni corrected p-values less than 0.05 (i.e., $p < 0.00625$, corrected for multiple comparisons across brain regions) were considered to be statistically significant. Post hoc statistical power (1- β) was calculated for each ROI measurement using G*Power 3.1 tool *[Heinrich Heine University of Dusseldorf, Germany]* (122).

3.4 Results:

The percent change maps for FA, MD, T_1, T_2 and MWF at different time points relative to the baseline (i.e. first time point) are shown in Figure 3-3 to visualize the spatiotemporal variations of

each quantitative MRI measure across the whole brain. To better understand the ROI-specific alterations, we calculated the changes in MRI measures (FA, MD, T_1, T_2 and MWF) over fixation time (in hours) for eight deep WM and GM structures, as shown in Figures 3-4 to 3-8 (which also show examples of FA, MD, T_1, T_2 and MWF maps). Corresponding correlation coefficients, p-values and post hoc statistical powers are presented in Table 3-2.

Overall, the diffusion imaging measurements appeared to be noisier, and perhaps in part because of this, less affected by formalin fixation than either relaxometry or myelin water measurements. We observed that FA values (Figure 3-4) were not significantly different in 6 out of 8 structures. In both subjects, Optic Radiation ($p = 9.6 \times 10^{-4}$ and $p = 0.001$) showed gradual, albeit statistically significant decreases, and Subject 1 and Subject 2 showed statistically significant increases in the Splenium of CC ($p = 3.8 \times 10^{-4}$) and Thalamus ($p = 0.001$) respectively. Similarly, no significant changes in MD values (Figure 3-5) were observed in 7 of 8 structures for both subjects. Subject 1 showed significant positive correlations in the Genu of the CC ($p = 0.003$), while Subject 2 showed strong negative correlations in the Thalamus ($p = 6.1 \times 10^{-4}$). As expected, however, FA and MD were anti-correlated, in that structure with higher FA had lower MD and vice versa. Moreover, the baseline (i.e., first time point) FA values in WM regions were higher than those in GM regions, as expected (39,87).

Table 3-2: *Subject-wise Spearman correlations between formalin fixation time and quantitative MRI values*[a]

			Genu of the CC	***Splenium of the CC***	***Internal Capsule***	***Optic Radiation***	***Caudate Nucleus***	***Globus Pallidus***	***Putamen***	***Thalamus***
FA	Subject 1	r_s	0.1	**-0.83**	0.1	**-0.8**	-0.01	0.32	0	0.19
		p-value	0.72	**<0.001**	0.73	**<0.001**	0.95	0.27	1	0.51
		Power	0.06	**0.99**	0.06	**0.99**	0.05	0.199	0.05	0.09
	Subject 2	r_s	-0.58	-0.51	-0.4	**-0.78**	0.14	0.25	-0.1	**0.78**
		p-value	0.03	0.07	0.17	**0.001**	0.62	0.39	0.72	**0.001**
		Power	0.647	0.496	0.3	**0.98**	0.075	0.136	0.06	**0.98**
MD	Subject 1	r_s	**0.73**	-0.19	0.5	-0.45	0.68	0.36	0.15	0.45
		p-value	**0.003**	0.51	0.08	0.12	0.009	0.21	0.61	0.11
		Power	**0.937**	0.097	0.475	0.381	0.86	0.246	0.079	0.381
	Subject 2	r_s	-0.41	-0.46	-0.34	-0.66	-0.14	-0.01	0.51	**-0.81**
		p-value	0.15	0.10	0.25	0.012	0.63	0.96	0.07	**<0.001**
		Power	0.31	0.399	0.22	0.82	0.075	0.05	0.496	**0.99**
T_1	Subject 1	r_s	**-0.98**	**-1**	**-1**	**-1**	**-0.98**	**-1**	**-1**	**-1**
		p-value	**$<10^{-7}$**	**0**	**0**	**0**	**$<10^{-7}$**	**0**	**0**	**0**
		Power	**1**	**1**	**1**	**1**	**1**	**1**	**1**	**1**
	Subject 2	r_s	**-0.97**	**-0.93**	**-1**	**-1**	**-0.83**	**-0.99**	**-0.98**	**-0.99**
		p-value	**$<10^{-7}$**	**$<10^{-5}$**	**0**	**0**	**<0.001**	**$<10^{-11}$**	**$<10^{-9}$**	**$<10^{-12}$**
		Power	**1**	**1**	**1**	**1**	**0.998**	**1**	**1**	**1**
T_2	Subject 1	r_s	**-0.96**	**-0.95**	**-0.97**	**-0.96**	**-0.97**	**-0.95**	**-0.94**	**-0.95**
		p-value	**$<10^{-7}$**	**$<10^{-7}$**	**$<10^{-8}$**	**$<10^{-7}$**	**$<10^{-7}$**	**$<10^{-6}$**	**$<10^{-6}$**	**$<10^{-7}$**
		Power	**1**	**1**	**1**	**1**	**1**	**1**	**1**	**1**
	Subject 2	r_s	**-0.70**	-0.008	**-0.95**	**-0.88**	0.18	**-0.86**	**-0.90**	**-0.86**
		p-value	**0.006**	0.97	**$<10^{-6}$**	**$<10^{-6}$**	0.55	**<0.001**	**<0.0001**	**<0.001**
		Power	**0.89**	0.05	**1**	**0.99**	0.092	**0.99**	**1**	**0.99**
MWF	Subject 1	r_s	**0.99**	**0.99**	**1**	**1**	**0.95**	**0.99**	**0.98**	**1**
		p-value	**$<10^{-11}$**	**$<10^{-11}$**	**0**	**0**	**$<10^{-11}$**	**$<10^{-11}$**	**$<10^{-9}$**	**0**
		Power	**1**	**1**	**1**	**1**	**1**	**1**	**1**	**1**
	Subject 2	r_s	0.89	**0.95**	**0.98**	**0.99**	0.39	**0.97**	**0.97**	**0.9**
		p-value	<0.01	**$<10^{-6}$**	**$<10^{-8}$**	**$<10^{-11}$**	0.18	**$<10^{-8}$**	**$<10^{-8}$**	**<0.001**

Power	0.99	**1**	**1**	**1**	0.286	**1**	**1**	**0.99**

[a]Correlations with $p < 0.00625$ (Bonferroni corrected) are highlighted with bold font. CC: Corpus Callosum.

For both subjects, the relaxation times (T_1 and T_2) were significantly affected by formalin fixation in all eight regions. T_1-relaxation times were reduced by 30-60% at the final time point compared to baseline, and these reductions were statistically significant in both WM and GM structures ($p \leq 10^{-4}$ in all cases) (Figure 3-6). Similarly, T_2-relaxation times appeared to be affected by progressive formalin fixation, with most regions showing significant negative correlations (Figure 3-7). However, T_2 was not significantly changed in the Splenium of the CC ($p = 0.97$) or Caudate Nucleus ($p = 0.55$) for Subject 2.

Finally, the apparent MWF exhibited significant increase in all eight WM and GM regions for Subject 1, and 7 out of 8 regions for Subject 2 (Figure 3-8). However, although the MWF in the Caudate Nucleus of Subject 2 did not produce a significant overall Spearman rank correlation ($p = 0.18$, due to the decreased later time-points, relative to the middle time-points), it should be noted that all of the MWF estimates beyond the third time-point (i.e., 24 hours) were still at least twice as large as the initial baseline value.

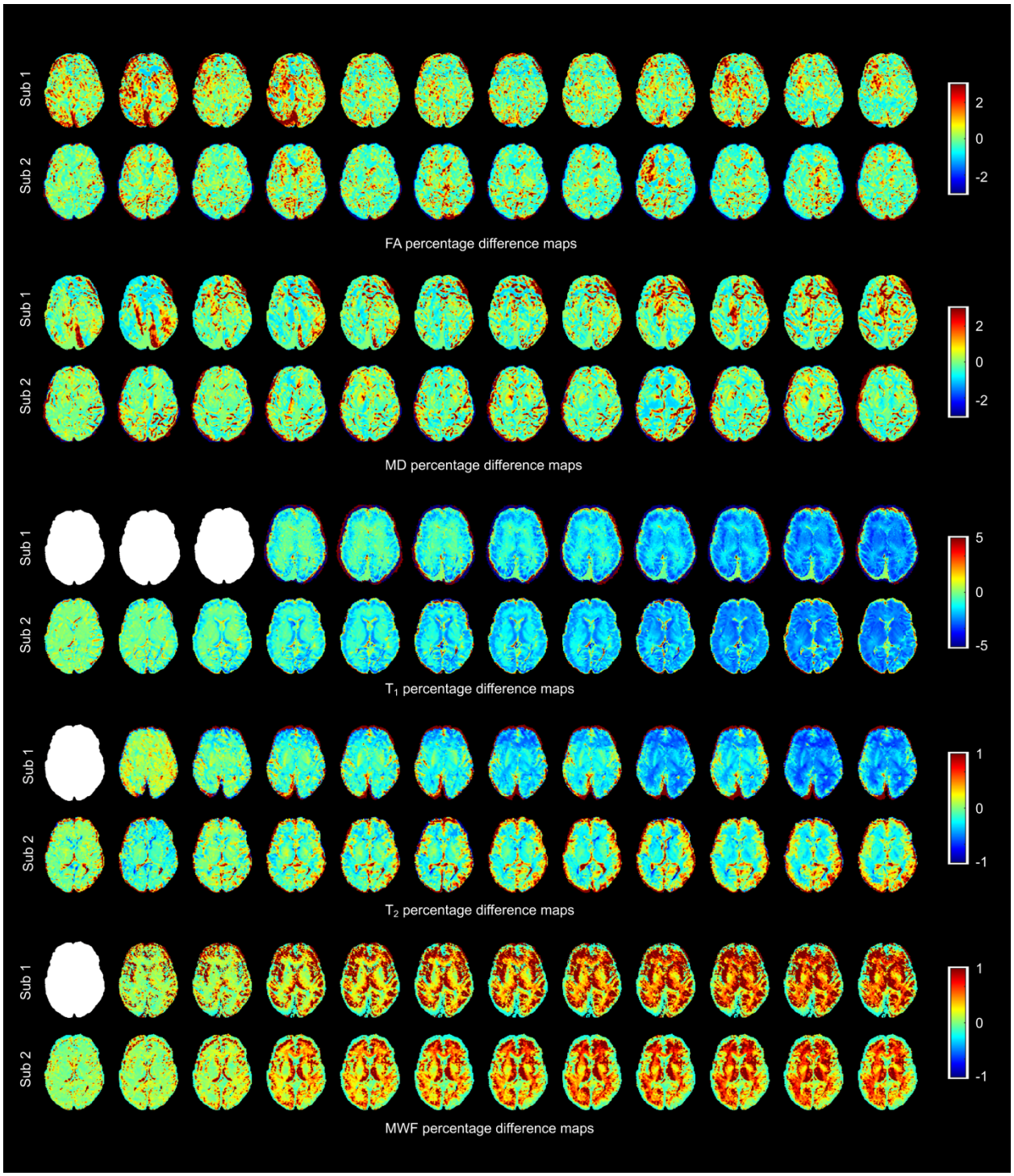

Figure 3-3: *Percentage difference maps of FD, MD, T_1, T_2 and MWF of each subject at 12, 24, 46, 120, 168, 211, 288, 336, 500, 672, 840 and 1032 hours after initial fixation compared to 0-hour scan. Due to substantial noise component at 0 hours, T_2 and MWF maps of Subject 1 was compared to the image obtained at 12 hours (i.e., time point 2). Due to MP2RAGE licensing issue, T_1 images of Subject 1 could not be obtained at 0, 12 and 24 hours and therefore, T_1 difference maps of Subject 1 were compared to 46-hour scan (time point 4). Blank images represent the missing maps.*

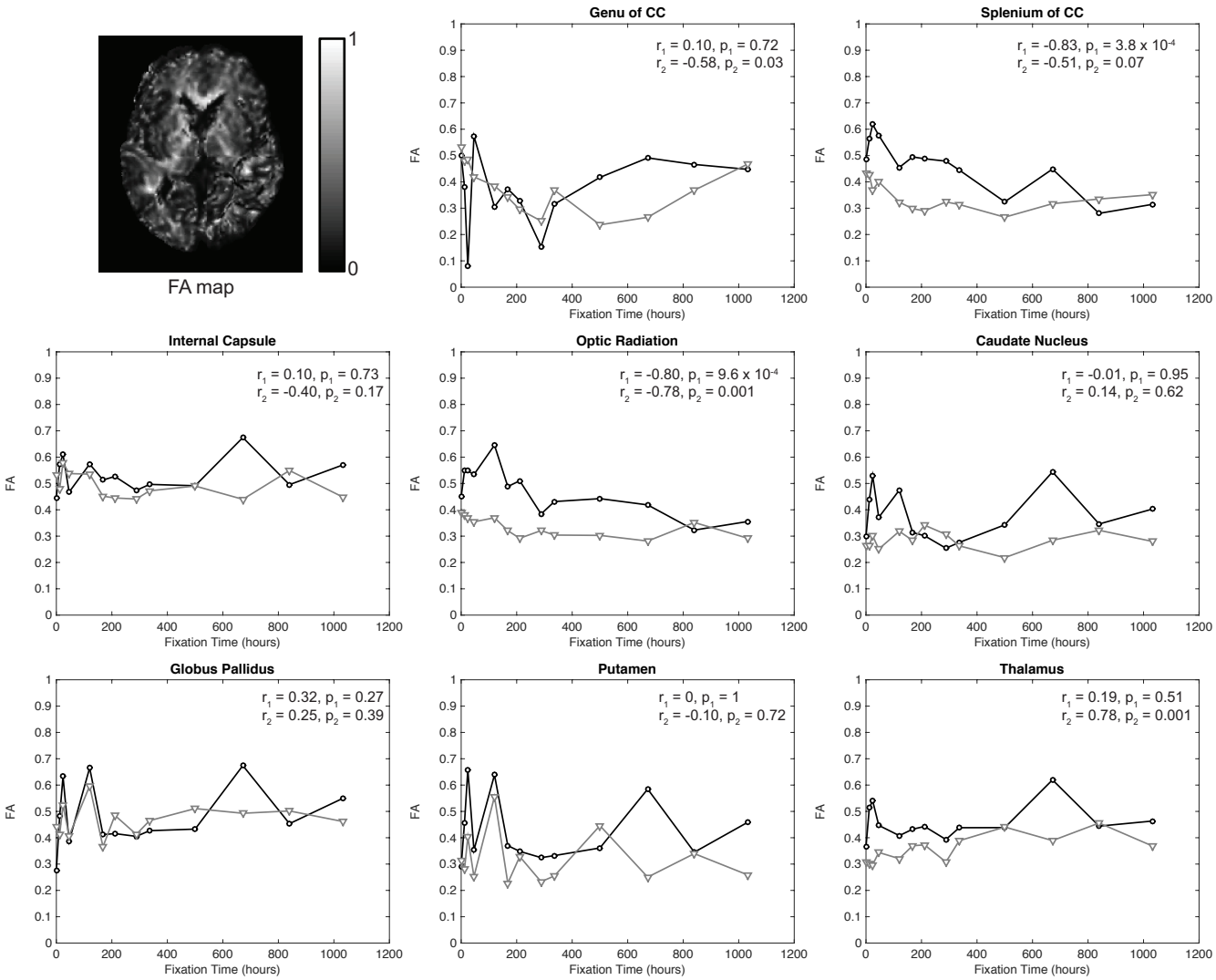

Figure 3-4: *FA vs. time of fixation are shown for eight structures (Genu of Corpus Callosum, Splenium of Corpus Callosum, Internal Capsule, Optic Radiation, Caudate Nucleus, Globus Pallidus, Putamen and Thalamus). The x-axis shows the time in hours, where x=0 is the time of first formalin immersion. The y-axis shows FA in each structure. The black and grey lines represent structures for Subject 1 and Subject 2 respectively. Plots show FA changes in each structure throughout the fixation. An example fractional anisotropy (FA) map from Subject 2 has been shown in the top left.*

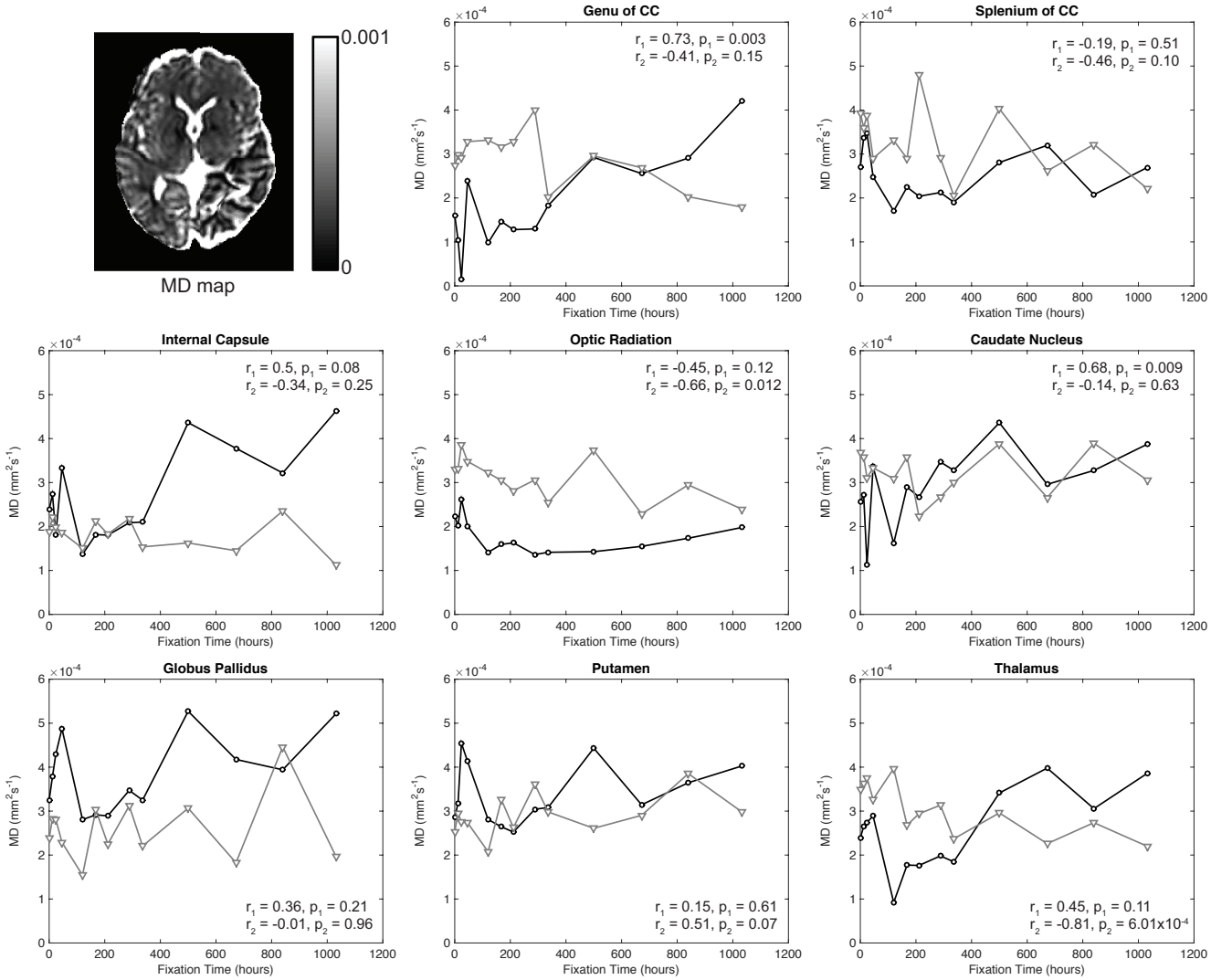

Figure 3-5: *MD vs. time of fixation are shown for eight structures (Genu of Corpus Callosum, Splenium of Corpus Callosum, Internal Capsule, Optic Radiation, Caudate Nucleus, Globus Pallidus, Putamen and Thalamus). The x-axis shows the time in hours, where x=0 is the time of first formalin immersion. The y-axis shows MD in each structure. The black and grey lines represent structures for Subject 1 and Subject 2 respectively. Plots show MD changes in each structure throughout the fixation. An example MD map from Subject 2 has been shown in the top left.*

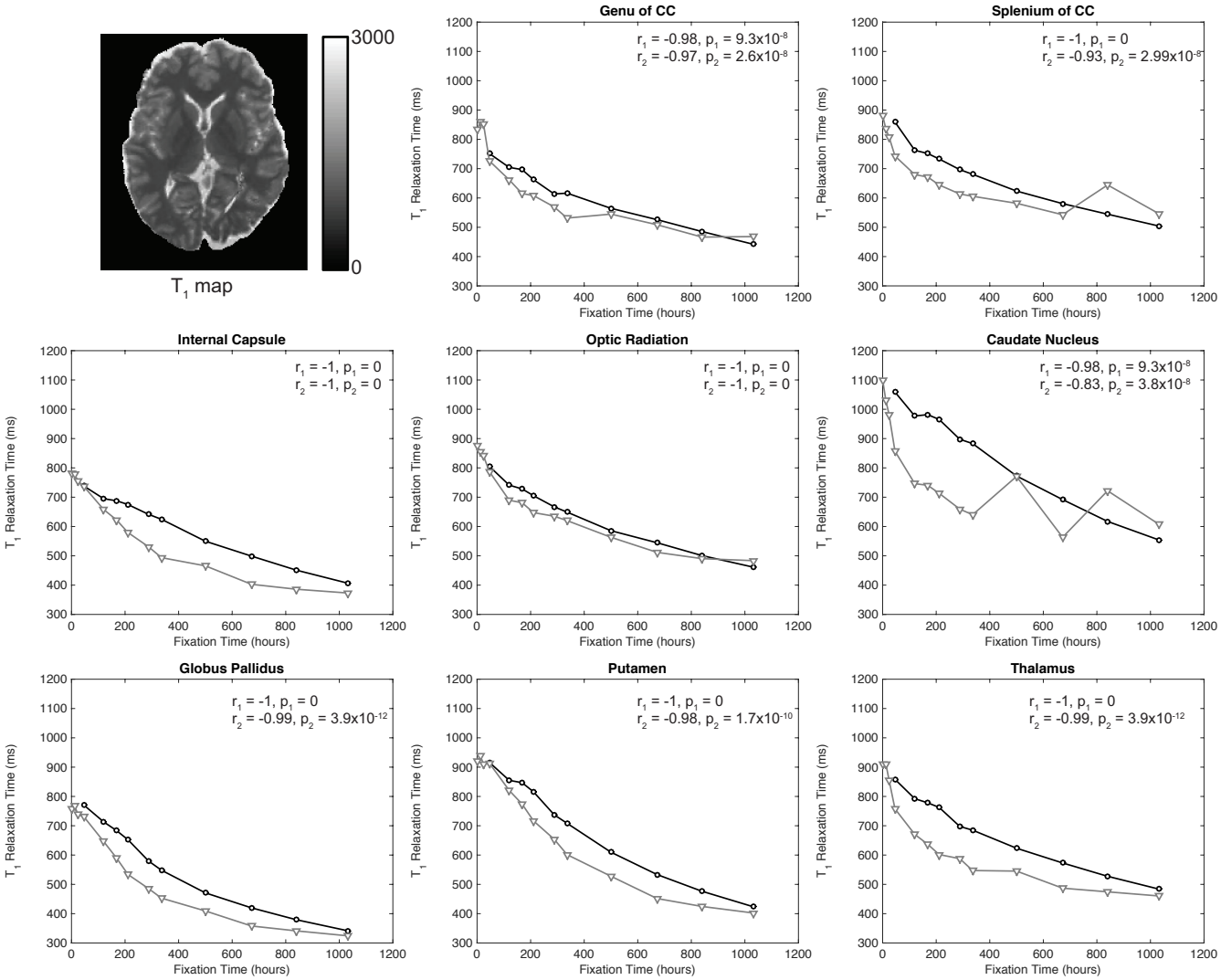

Figure 3-6: *T_1 vs. time of fixation are shown for eight structures (Genu of Corpus Callosum, Splenium of Corpus Callosum, Internal Capsule, Optic Radiation, Caudate Nucleus, Globus Pallidus, Putamen and Thalamus). The x-axis shows the time in hours, where x=0 is the time of first formalin immersion. The y-axis shows T_1 in each structure. The black and grey lines represent structures for Subject 1 and Subject 2 respectively. Plots show T_1 changes in each structure throughout the fixation. An example T_1 map from Subject 2 has been shown in the top left.*

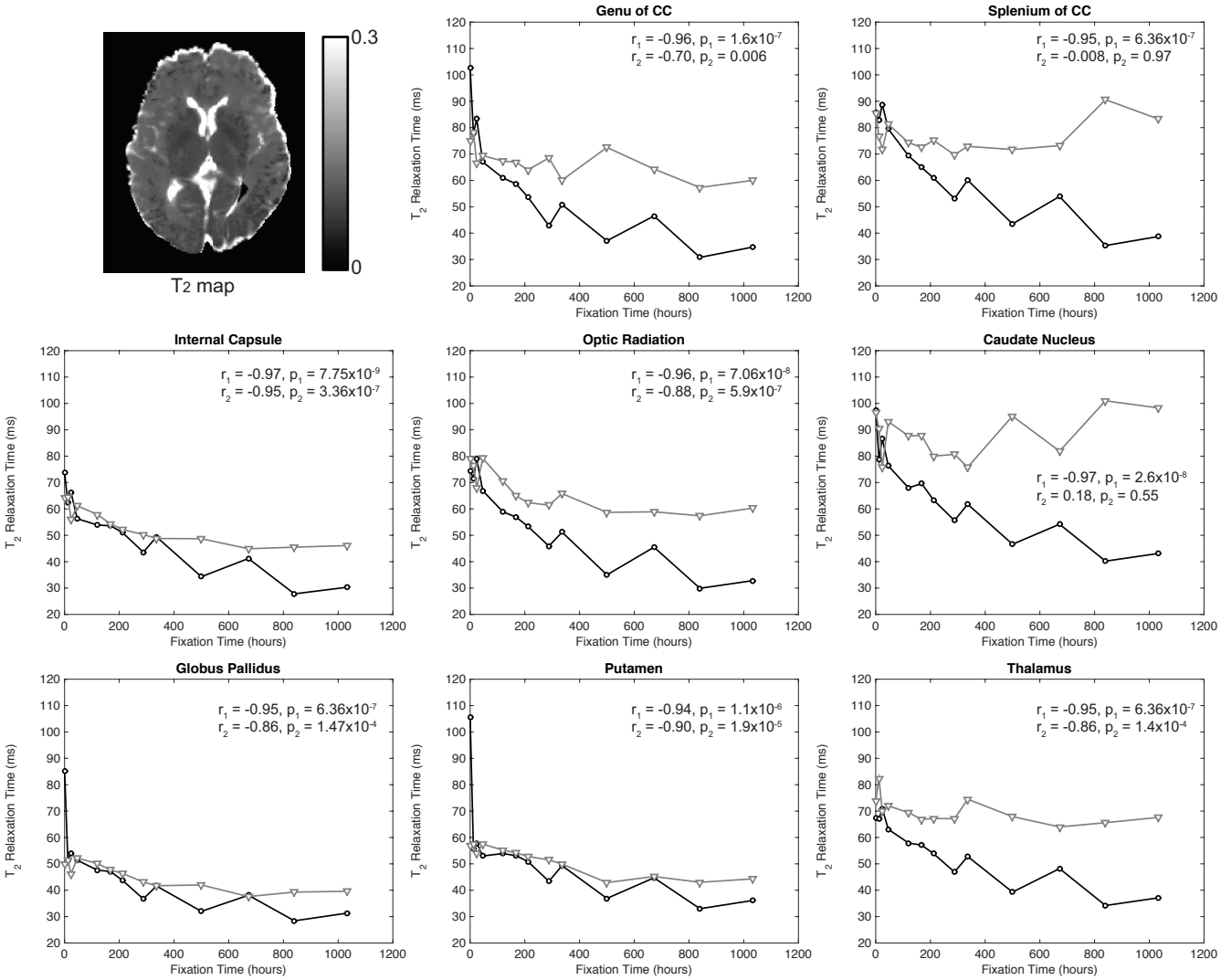

Figure 3-7: *T_2 vs. time of fixation are shown for eight structures (Genu of Corpus Callosum, Splenium of Corpus Callosum, Internal Capsule, Optic Radiation, Caudate Nucleus, Globus Pallidus, Putamen and Thalamus). The x-axis shows the time in hours, where x=0 is the time of first formalin immersion. The y-axis shows T_2 in each structure. The black and grey lines represent structures for Subject 1 and Subject 2 respectively. Plots show T_2 changes in each structure throughout the fixation. An example T_2 map from Subject 2 has been shown in the top left.*

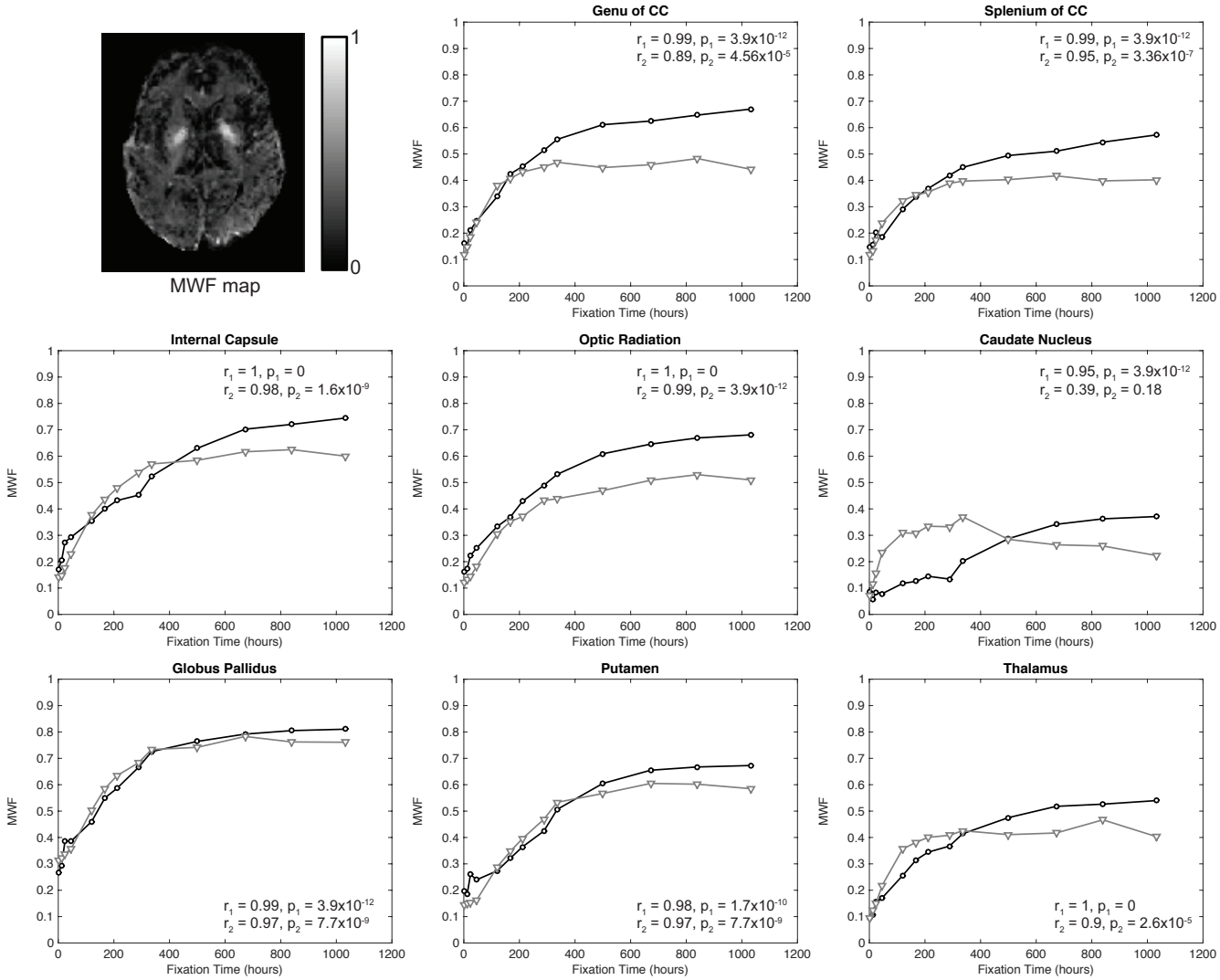

Figure 3-8: *MWF vs. time of fixation are shown for eight structures (Genu of Corpus Callosum, Splenium of Corpus Callosum, Internal Capsule, Optic Radiation, Caudate Nucleus, Globus Pallidus, Putamen and Thalamus). The x-axis shows the time in hours, where x=0 is the time of first formalin immersion. The y-axis shows MWF in each structure. The black and grey lines represent structures for Subject 1 and Subject 2 respectively. Plots show MWF changes in each structure throughout the fixation. An example MWF map from Subject 2 has been shown in the top left.*

3.5 Discussion:

We have demonstrated the time-dependent effects of formalin fixation on various quantitative MRI measurements (i.e., FA, MD, T_1, T_2 and MWF) throughout whole human brain samples, and have characterized these changes in several WM and GM tissue structures. We found that formalin fixation did not systematically effect diffusion measurements (FA and MD values) as significantly as other quantitative measures: namely, T_1-relaxation times, T_2-relaxation times and MWF estimates, which were progressively altered by tissue fixation.

Although the overall FA and MD changes were not significantly correlated with formalin fixation time, we observed large signal fluctuations between consecutive scans (Figures 3-4 and 3-5), which suggests that there were issues with either: 1) the preprocessing (e.g., co-registration, spatial normalization, etc.), or 2) the contrast-to-noise ratio (CNR) of the diffusion maps. Given that the same preprocessing pipeline and spatial normalization parameters were used for the diffusion data and the rest of the contrast maps (which did not show similar fluctuations), we suspect that the underlying cause of these instabilities are more likely related to the reduced CNR associated with ex vivo diffusion imaging. For example, the ~15°C differential between room temperature (~22 °C) and body temperature (~37 °C) means that the actual amount of water diffusion is reduced compared to in vivo conditions (all else being equal). Moreover, as T_2-relaxation times are decreased with progressive fixation (Figure 3-7), ostensibly 'diffusion weighted' images will become increasingly dominated by T_2-weighting. As a result, using 'standard' in vivo diffusion-encoding parameters (e.g., b = 700 s/mm^2 and TE > 70 ms, as used in the current experiment) is expected to produce lower CNR for diffusion measurements. Unfortunately, as pointed out in previous ex vivo diffusion imaging studies using even lower b-values (78), increased diffusion-

encoding sensitivity comes at the expense of signal-to-noise ratio (SNR) (123), so using higher b-values would need to be offset by other data acquisition parameters (e.g., higher field strength, longer scan times, etc.) that were not possible in the current experiment.[2] Nonetheless, a strong FA vs. fixation time correlation ($r_1 = -0.8$, $p_1 = 9.6 \times 10^{-4}$; $r_2 = -0.78$, $p_2 = 0.001$) was observed in the optic radiation for both subjects. This fiber bundle has higher myelin density than the surrounding tissue (124), which may partially explain the higher directional anisotropy (and higher CNR) compared to other structures.

Consistent with other previous studies (13,15,17,28,58–61), T_1-relaxation times decreased with time of formalin fixation for all structures. These T_1 changes may be a result of the viscosity of the fixation media, radius, spin-spin distance of molecules and protein cross-linking as described by an earlier study (125). Compared with T_1 changes, the T_2 shortening appeared to be slower, but these changes were still highly significant, and were similar to earlier studies (77–79). Though the mechanisms are not known, increased tissue rigidity due to formalin-induced protein cross-linking may play a role in T_2 shortening as well. One previous study has mentioned the possibility of interactions between myelin lipids and water molecules inside the tissue compartments (46), while another study suggested that an altered 'exchange diffusion rate' between free and bound water molecules may play a role (110). Additionally, tissue dehydration (77,83) and replacement of formalin solution at regular intervals are thought to have T_1 and T_2 shortening effects (126).

[2] It is worth noting that stronger diffusion-encoding gradients, allowing higher b-values and/or shorter TEs, might be particularly effective for future *ex vivo* diffusion experiments, since these would maximize both SNR and diffusion CNR (all else being equal), without having to worry about neurostimulation, which places practical limits on the maximum gradient strength that can be used for *in vivo* diffusion imaging.

In stark contrast to relaxometry measures, the MWF values increased rapidly and all regions showed highly significant positive correlations with fixation time – with the exception of the Genu of CC and Caudate Nucleus for Subject 2. To the best of our knowledge, this is the first study to investigate relationships between MWF measurements and tissue fixation, and the exact mechanisms underlying these MWF changes are not clearly understood. However, we speculate that tissue dehydration is again likely to play a key role, where a reduction of intra- and extra-cellular water (53) in brain tissue - most likely due to the chemical reaction between water and refilled formalin (109) – would artificially inflate apparent MWF values by reducing the denominator (i.e. myelin plus intra/extra-cellular water) in the MWF equation. Our T_2 shortening values arising from the intra/extra-cellular water components tend to support this notion, although further investigation is required to support this theory and to understand the exact cause(s) for these MRI changes. Nonetheless, our findings clearly indicate that even small differences in fixation time between tissue samples could have large effects on the measurements, and that researchers must exercise extreme caution when comparing in vivo MWF values with ex vivo values.

Despite our best efforts to optimize the experimental design, acquisition and analysis, there are a few noteworthy limitations in this study (in addition to the challenges mentioned above regarding the ex vivo diffusion measurements). Due to ethical and logistical constraints (e.g., BREB approval, patient consent, availability of neurologically-healthy adult brain specimens, autopsy scheduling, and availability of MRI scanner time) our sample size was small (n = 2) and PMIs were not as short or consistent as desired (in order to inspect the immediate postmortem changes). Therefore, differences in PMI (i.e., 33 hours vs. 55 hours) may have had an effect on the results,

as PMI is known to affect MR properties (31,35,86). Partial volume effects due to tissue segmentation, subcortical structures adjacent to formalin, and imperfect spatial normalizations to the MNI template may have affected quantitative precision in MRI measures. Furthermore, despite the fact that other studies suggest that tissue fixation continues to change MRI properties up to 1142 hours (127) or even a year (81), we were unable to evaluate the MRI changes beyond 1032 hours in our study because the samples had to undergo neuropathological examinations for diagnostic purposes at that time (in accordance with standard neuropathology practices at our site, and in accordance with our BREB approval). T_2 relaxometry was performed using multi-echo 3D GRASE images from the myelin water imaging sequence, which used a relatively short TR that introduces more T_1-weighting than traditional T_2 relaxometry methods. However, we did not have enough time in each session to acquire separate T_2 relaxometry data, and since the amount of T_1-weighting was constant across samples and time-points, these effects are thought to be minimal. Nonetheless, since significant T_1-relaxation changes were identified, there may have been some interaction between T_1 and T_2 effects in the T_2 relaxometry data.

At least one previous study noted that the position of the tissue in formalin should be taken into consideration while characterizing longitudinal effects of fixation (79); however, our plastic container was filled by formalin so that the whole cortical surface had uniform contact with formalin for the entire study duration. Furthermore, our whole-brain maps of the spatiotemporal changes suggest that tissue fixation occurred evenly, as the formalin perfused deeper into the tissue over time, eventually penetrating deep into each of the brain specimens.

Finally, considering the relatively low cost of the fixation and imaging protocols employed in the current study, these practices should be highly adoptable not only for future research applications, but also in forensic autopsy practice, since it provides high quality images with a number of different tissue contrasts within a clinically acceptable timeframe.

3.6 Conclusions:

In this study, we characterized the time-dependent effects of formalin fixation on FA, MD, T_1-relaxation, T_2-relaxation and MWF values in whole postmortem human brains. The T_1, T_2 and MWF changes indicate that formalin gradually diffuses inward from the cortical surface, and tissue fixation continues to affect MR properties until (and perhaps beyond) our maximum fixation time of 1032 hours. Our results lead to the conclusion that ex vivo relaxometry (T_1 and T_2) mapping and myelin water imaging should be performed immediately after formalin fixation (to avoid erroneous signals), while ex vivo diffusion imaging measures (FA and MD) appear to be more affected by other factors (e.g., temperature), even after prolonged fixation

3.7 Acknowledgements:

The authors acknowledge funding from The University of Manitoba (UofM), The Natural Sciences and Engineering Research Council of Canada (NSERC), The Winnipeg Health Sciences Centre Foundation (HSCF), and Brain Canada. The authors would also like to thank the Radiology Research Coordinator (Teresa Figley) and the MRI Technologists (particularly Paul Barrette, Laura Garry, Brandi Adolphe, Mike Gordillo, Cynthia Kulczycki, Caitlin Gallant, Cindy Storey, and Alexi Thiessen) at the Winnipeg Health Sciences Centre for helping with the MRI scheduling

and data acquisition, and the following Autopsy Technical Assistants at the Department of Pathology (Samuel Findlay, Chris Kacsmar, Terry Beach, Cheryl Fernando, and Marvin Mayuga) at the Winnipeg Health Sciences Centre for their assistance in procuring and preserving the brain specimens. We would also like to extend special thanks to the developers of the MP2RAGE sequence (Drs. Tobias Kober and Bénédicte Maréchal at Siemens) for kindly sharing their work-in-progress (WIP) package with us.

Chapter 4 : General Discussion and Future Directions

4.1 Discussion

Postmortem MRI presents an opportunity for neuroradiologists and neuropathologists to investigate brain structure and microstructure non-invasively, and in more detail than can be achieved in vivo. Ex vivo imaging can reveal various structural inconsistencies that may have remained undetected during routine autopsy and may prove to be a useful modality for future postmortem analyses, as well as for generating disease-specific information (such as mortality-statistics). The objectives of this thesis were to find a cost effective and artefact-free method to conduct whole brain ex vivo MRI studies with clinical MRI systems and to map spatiotemporal changes of various quantitative MRI measures resulting from progressive formalin fixation. In addition to the longitudinal characterization of formalin-affected MRI properties, this study also responded to the two fundamental clinical issues: firstly, if postmortem 'whole-brain' imaging can provide a closer approximation to its in vivo status and secondly, if the whole process is clinically applicable.

Chapter 2 presented an affordable, easy and time saving method to obtain cavity and artifact-free high resolution images. This will provide a standard procedure for future researchers to conduct single time-point of longitudinal ex vivo brain MRI studies. By following our method, it was observed that, the formalin band was clearly visible in the T_1-weighted images (both from MPRAGE and MP2RAGE), but not in other images (i.e. T_2, FA, MD, MWF) and, the band disappeared in later time points in T_1-weighted images. Furthermore, FA images showed weak

gray-white contrast, whereas the contrast in MD images was relatively strong. Although, the reasons for formalin band invisibility or the relative contrasts in DTI images are not clearly understood yet, penetration of formalin was visible deep into the brain. Several studies have attempted to reverse the contrast and MR changes by rehydrating the fixed tissue, for example, used agarose gel (82), phosphate buffered solution (PBS) (81), Fomblin (Solvay Solexis Inc.) (35,40,64,65) or gadolinium-doped buffer solution (64) and scanned the formalin-fixed specimen, but, such approaches for whole brain not only takes longer scan times (approximately from 40 min to 14 hours), but also, are costly and may not be practical to be applied in routine autopsy examination. Our formalin-only protocol (Chapter 2) took roughly 2 hours including sample preparation and MRI scan, without any apparent image degradation and artefacts. Thus, our fixation and imaging approach are highly adoptable within acceptable time frame for routine autopsy examination. However, offline image processing may be another area of concern for ex vivo MRI and should be given ample consideration. As advanced MRI hardware and sequences produce high resolution 3D data and contain plenty of information, it requires good computational resources that are able to perform image processing within a reasonable time.

In Chapter 3, the correlations between fixation time and different MR properties (i.e., FA, MD, T_1, T_2, MWF) were established and the results indicated that, T_1, T_2 and MWF images might not reflect the antemortem values if measured after prolonged fixation, and FA and MD values may be affected by other factors (i.e., temperature). In addition to the discussion and limitations reviewed in previous chapters, postmortem interval (PMI- the time between death and beginning of fixation) and scan interval (SI- the time between death and beginning of fixation) are two critical concerns that researchers should be cautious about. Earlier studies have mentioned that, ex vivo imaging of

fixed human brains is sensitive to PMI (39,64,83) and SI (79). Longer PMI has been reported to reduce FA (31,84), and MD (31,35) likely due to tissue decomposition (81), whereas SI based effects are due to increasing acidity (85), dehydration (83) and protein cross-linking (64,86). As there was no time delay between the brain immersion and scanning, it can be undertaken that, SI did not have any influence on the results of the baseline scans (time = 0 hours).

In the current studies, only neurologically healthy cases were examined. However, unforeseen situations such as hypoxic episodes, hemorrhage, hypoperfusion or intracranial pressure (35) may be a critical factor to study cases with underlying pathology, but it should not be a major confining issue for cases without neurological disorders, as presented in this study. Additionally, a previous study indicated that the position of formalin surrounding the surface should be taken into consideration while characterizing the longitudinal effect of fixation (79). As our plastic container was filled by formalin in full and there was no formalin leak during the entire study period, the whole cortical surface had uniform contact with formalin for the entire study time. Despite the limitations described so far, I believe that, the thesis has succeeded in achieving the objectives as outlined in Chapter 1 and I also hope that, future directions will lead this study into further explorations.

4.2 Future Directions

As discussed earlier, the MR properties such as FA and MD are sensitive to PMI and it is not known if other MR properties are affected, hence reducing the PMI less than 33 hours may be an area to improve and then, one can observe if it significantly changes our findings. Due to logistical

issues, it was not possible to obtain more than 2 samples during the timeframe of this research. Although findings were generally quite consistent between subjects, a higher number of subjects (at least 3 to 5) from non-neurological cases and more ROIs with a longer study period will be able to validate our findings and such data might allow for mathematical modelling so that, prediction at any time-point can be achieved.

With histopathology correlation, this study can be re-applied on diseased autopsy brains from neurodegenerative disorders and will validate emerging novel MRI techniques. MWF is a prime example, which is promising for future clinical application in demyelinating diseases, especially for MS. Nearly 100,000 Canadians aged between 20 and 40 years are affected by Multiple Sclerosis (MS). It is a heterogeneous neurological disorder, clinical diagnosis for which requires demonstration of multiple CNS lesions separated in time (temporal heterogeneity) and space (spatial heterogeneity). Therefore, neuroimaging, especially, MRI has been playing a pivotal role in clinical management as an imaging biomarker. By validating with histopathology, MWF has potential to become a reliable biomarker for MS patients. Our approach involving ex vivo MRI of autopsy brains can offer radiology-pathology correlation to verify MWF to study underlying pathology mechanisms. Not only with common histology staining methods like Luxol fast blue, Bielschowsky staining etc. (128), but also correlations can be expanded to include proteomic profiling for myelin-associated proteins, such as myelin basic protein (MBP), proteolipid protein (PLP), or myelin-associated glycoprotein (MAG). To the best of our knowledge, such studies have not been reported yet. We expect that this will help us to understand the detailed myelinated fiber architecture at the cellular or molecular level. Thus, an extension to our research may play a major role in establishing a comprehensive radiology-pathology approach, which I anticipate to have a

great clinical value and may ultimately help to test/validate therapeutic strategies for clinical application.

References:

1. Shatil AS, Matsuda KM, Figley CR, Medicine A, Centre HS, Sciences B. A Method for Whole Brain Ex Vivo Magnetic Resonance Imaging with Minimal Susceptibility Artifacts. Front. Neurol. 2016. doi: 10.3389/fneur.2016.00208.

2. Prasad P V. Magnetic Resonance Imaging Methods and Biologic Applications. Totowa, NJ: Humana Press Inc.; 2006. doi: 10.1385/1597450103.

3. Brown R. XXVII. A brief account of microscopical observations made in the months of June, July and August 1827, on the particles contained in the pollen of plants; and on the general existence of active molecules in organic and inorganic bodies. Philos. Mag. Ser. 2 1828;4:161–173. doi: 10.1080/14786442808674769.

4. Moseley ME, Cohen Y, Kucharczyk J, Mintorovitch J, Asgari HS, Wendland MF, Tsuruda J, Norman D. Diffusion-weighted MR imaging of anisotropic water diffusion in cat central nervous system. Radiology 1990;176:439–45. doi: 10.1148/radiology.176.2.2367658.

5. Chenevert TL, Brunberg J a, Pipe JG. Anisotropic diffusion in human white matter: demonstration with MR techniques in vivo. Radiology 1990;177:401–405. doi: 10.1148/radiology.177.2.2217776.

6. Basser PJ, Mattiello J, Lebihan D. Estimation of the Effective Self-Diffusion Tensor from the NMR Spin Echo. J. Magn. Reson. Ser. B 1994;103:247–254. doi: 10.1006/jmrb.1994.1037.

7. Basser PJ, Mattiello J, LeBihan D. MR diffusion tensor spectroscopy and imaging. Biophys. J. 1994;66:259–67. doi: 10.1016/S0006-3495(94)80775-1.

8. Pierpaoli C, Jezzard P, Basser PJ, Barnett a, Di Chiro G. Diffusion tensor MR imaging of the human brain. Radiology 1996;201:637–648. doi: 10.1148/radiology.201.3.8939209.

9. Song S-K, Sun S-W, Ramsbottom MJ, Chang C, Russell J, Cross AH. Dysmyelination Revealed

through MRI as Increased Radial (but Unchanged Axial) Diffusion of Water. Neuroimage 2002;17:1429–1436. doi: 10.1006/nimg.2002.1267.

10. Hagmann P, Jonasson L, Maeder P, Thiran JP, Wedeen VJ, Meuli R. Understanding diffusion MR imaging techniques: from scalar diffusion-weighted imaging to diffusion tensor imaging and beyond. Radiographics 2006;26 Suppl 1:S205-23. doi: 10.1148/rg.26si065510.

11. Koay CG, Chang LC, Carew JD, Pierpaoli C, Basser PJ. A unifying theoretical and algorithmic framework for least squares methods of estimation in diffusion tensor imaging. J. Magn. Reson. 2006;182:115–125. doi: 10.1016/j.jmr.2006.06.020.

12. Sundgren PC, Dong Q, Gómez-Hassan D, Mukherji SK, Maly P, Welsh R. Diffusion tensor imaging of the brain: Review of clinical applications. Neuroradiology 2004;46:339–350. doi: 10.1007/s00234-003-1114-x.

13. Mori S, Zhang J. Principles of Diffusion Tensor Imaging and Its Applications to Basic Neuroscience Research. Neuron 2006;51:527–539. doi: 10.1016/j.neuron.2006.08.012.

14. Le Bihan D, Mangin JF, Poupon C, Clark C a, Pappata S, Molko N, Chabriat H. Diffusion tensor imaging: concepts and applications. J. Magn. Reson. Imaging 2001;13:534–546. doi: 10.1002/jmri.1076 [pii].

15. Moseley M, Bammer R, Illes J. Diffusion-tensor imaging of cognitive performance. Brain Cogn. 2002;50:396–413. doi: 10.1016/S0278-2626(02)00524-9.

16. Vilanova A, Zhang S, Kindlmann G, Laidlaw D. An introduction to visualization of diffusion tensor imaging and its applications. Vis. Appl. DTI 2006:121–153. doi: 10.1007/3-540-31272-2_7.

17. Nucifora PGP, Verma R, Lee S-K, Melhem ER. Diffusion-tensor MR imaging and tractography: exploring brain microstructure and connectivity. Radiology 2007;245:367–384. doi:

10.1148/radiol.2452060445.

18. Ciccarelli O, Catani M, Johansen-Berg H, Clark C, Thompson A. Diffusion-based tractography in neurological disorders: concepts, applications, and future developments. Lancet Neurol. 2008;7:715–727. doi: 10.1016/S1474-4422(08)70163-7.

19. Johansen-Berg H, Behrens TEJ. Diffusion MRI: From quantitative measurement to in-vivo neuroanatomy. 2009. doi: 10.1016/B978-0-12-374709-9.00002-X.

20. Madden DJ, Bennett IJ, Song AW. Cerebral white matter integrity and cognitive aging: Contributions from diffusion tensor imaging. Neuropsychol. Rev. 2009;19:415–435. doi: 10.1007/s11065-009-9113-2.

21. Yamada K, Sakai K, Akazawa K, Yuen S, Nishimura T. MR Tractography: A Review of Its Clinical Applications. Magn. Reson. Med. Sci. 2009;8:165–174. doi: 10.2463/mrms.8.165.

22. Chanraud S, Zahr N, Sullivan E V., Pfefferbaum A. MR diffusion tensor imaging: A window into white matter integrity of the working brain. Neuropsychol. Rev. 2010;20:209–225. doi: 10.1007/s11065-010-9129-7.

23. de Carvalho Rangel C, Hygino Cruz LC, Takayassu TC, Gasparetto EL, Domingues RC. Diffusion MR imaging in central nervous system. Magn. Reson. Imaging Clin. N. Am. 2011;19:23–53. doi: 10.1016/j.mric.2010.10.006.

24. Fung SH, Roccatagliata L, Gonzalez RG, Schaefer PW. MR Diffusion Imaging in Ischemic Stroke. Neuroimaging Clin. N. Am. 2011;21:345–377. doi: 10.1016/j.nic.2011.03.001.

25. Hygino da Cruz LC, Vieira IG, Domingues RC. Diffusion MR Imaging: An Important Tool in the Assessment of Brain Tumors. Neuroimaging Clin. N. Am. 2011;21:27–49. doi: 10.1016/j.nic.2011.01.010.

26. Thomason ME, Thompson PM. Diffusion Imaging, White Matter, and Psychopathology.

Annu. Rev. Clin. Psychol. 2011;7:63–85. doi: 10.1146/annurev-clinpsy-032210-104507.

27. Voineskos AN, Rajji TK, Lobaugh NJ, Miranda D, Shenton ME, Kennedy JL, Pollock BG, Mulsant BH. Age-related decline in white matter tract integrity and cognitive performance: A DTI tractography and structural equation modeling study. Neurobiol. Aging 2012;33:21–34. doi: 10.1016/j.neurobiolaging.2010.02.009.

28. White T, Nelson M, Lim KO. Diffusion tensor imaging in psychiatric disorders. Top. Magn. Reson. Imaging 2008;19:97–109. doi: 10.1097/RMR.0b013e3181809f1e.

29. Budde MD, Xie M, Cross AH, Song SK. Axial diffusivity is the primary correlate of axonal injury in the experimental autoimmune encephalomyelitis spinal cord: a quantitative pixelwise analysis. J Neurosci 2009;29:2805–2813. doi: 10.1523/JNEUROSCI.4605-08.2009.

30. Gupta RK, Awasthi R, Rathore RKS, Verma A, Sahoo P, Paliwal VK, Prasad KN, Pandey CM, Narayana PA. Understanding epileptogenesis in calcified neurocysticercosis with perfusion MRI. Neurology 2012;78:618–625. doi: 10.1212/WNL.0b013e318248deae.

31. Schmierer K, Wheeler-Kingshott CAM, Boulby PA, Scaravilli F, Altmann DR, Barker GJ, Tofts PS, Miller DH. Diffusion tensor imaging of post mortem multiple sclerosis brain. Neuroimage 2007;35:467–477. doi: 10.1016/j.neuroimage.2006.12.010.

32. Guilfoyle DN, Helpern J a., Lim KO. Diffusion tensor imaging in fixed brain tissue at 7.0 T. NMR Biomed. 2003;16:77–81. doi: 10.1002/nbm.814.

33. Verma R, Mori S, Shen D, Yarowsky P, Zhang J, Davatzikos C. Spatiotemporal maturation patterns of murine brain quantified by diffusion tensor MRI and deformation-based morphometry. Proc Natl Acad Sci USA 2005;102:6978–6983. doi: 10.1073/pnas.0407828102.

34. Kroenke CD, Bretthorst GL, Inder TE, Neil JJ. Diffusion MR imaging characteristics of the developing primate brain. Neuroimage 2005;25:1205–1213. doi:

10.1016/j.neuroimage.2004.12.045.

35. D'Arceuil H, de Crespigny A. The effects of brain tissue decomposition on diffusion tensor imaging and tractography. Neuroimage 2007;36:64–68. doi: 10.1016/j.neuroimage.2007.02.039.

36. D'Arceuil H, Liu C, Levitt P, Thompson B, Kosofsky B, de Crespigny A. Three-Dimensional High-Resolution Diffusion Tensor Imaging and Tractography of the Developing Rabbit Brain. Dev. Neurosci. 2008;30:262–275.

37. Dyrby TB, Baaré WFC, Alexander DC, Jelsing J, Garde E, Søgaard L V. An ex vivo imaging pipeline for producing high-quality and high-resolution diffusion-weighted imaging datasets. Hum. Brain Mapp. 2011;32:544–563. doi: 10.1002/hbm.21043.

38. Tyszka JM, Frank LR. High-field diffusion MR histology: Image-based correction of Eddy-current ghosts in diffusion-weighted rapid acquisition with relaxation enhancement (DW-RARE). Magn. Reson. Med. 2009;61:728–733. doi: 10.1002/mrm.21876.

39. Miller KL, Stagg CJ, Douaud G, et al. Diffusion imaging of whole, post-mortem human brains on a clinical MRI scanner. Neuroimage 2011;57:167–181. doi: 10.1016/j.neuroimage.2011.03.070.

40. Miller KL, McNab J a., Jbabdi S, Douaud G. Diffusion tractography of post-mortem human brains: Optimization and comparison of spin echo and steady-state free precession techniques. Neuroimage 2012;59:2284–2297. doi: 10.1016/j.neuroimage.2011.09.054.

41. McNab JA, Jbabdi S, Deoni SCL, Douaud G, Behrens TEJ, Miller KL. High resolution diffusion-weighted imaging in fixed human brain using diffusion-weighted steady state free precession. Neuroimage 2009;46:775–785. doi: 10.1016/j.neuroimage.2009.01.008.

42. Birkl C, Langkammer C, Haybaeck J, Ernst C, Stollberger R, Fazekas F, Ropele S. Temperature-induced changes of magnetic resonance relaxation times in the human brain: A

postmortem study. Magn. Reson. Med. 2014;71:1575–1580. doi: 10.1002/mrm.24799.

43. Stewart WA, MacKay AL, Whittall KP, Moore GRW, Paty DW. Spin-Spin Relaxation in Experimental Allergic Encephalomyelitis. Analysis of CPMG Data Using a Non-Linear Least Squares Method and Linear Inverse Theory. Magn Reson Med 1993;29:767–75. doi: 10.1002/mrm.1910290608.

44. Wilhelm MJ, Ong HH, Wehrli SL, Li C, Tsai P-H, Hackney DB, Wehrli FW. Direct magnetic resonance detection of myelin and prospects for quantitative imaging of myelin density. Proc. Natl. Acad. Sci. 2012;109:9605–9610. doi: 10.1073/pnas.1115107109.

45. Brück W, Bitsch A, Kolenda H, Brück Y, Stiefel M, Lassmann H. Inflammatory central nervous system demyelination: Correlation of magnetic resonance imaging findings with lesion pathology. Ann. Neurol. 1997;42:783–793. doi: 10.1002/ana.410420515.

46. Laule C, Vavasour IM, Kolind SH, Li DKB, Traboulsee TL, Moore GRW, MacKay AL. Magnetic Resonance Imaging of Myelin. Neurotherapeutics 2007;4:460–484. doi: 10.1016/j.nurt.2007.05.004.

47. Beaulieu C. The basis of anisotropic water diffusion in the nervous system - A technical review. NMR Biomed. 2002;15:435–455. doi: 10.1002/nbm.782.

48. Wolff SD, Balaban RS. Magnetization transfer contrast (MTC) and tissue water proton relaxation in vivo. Magn. Reson. Med. 1989;10:135–144. doi: 10.1002/mrm.1910100113.

49. Gareau PJ, Rutt BK, Karlik SJ, Mitchell JR. Magnetization transfer and multicomponent T2 relaxation measurements with histopathologic correlation in an experimental model of MS. J. Magn. Reson. Imaging 2000;11:586–595. doi: 10.1002/1522-2586(200006)11:6<586::AID-JMRI3>3.0.CO;2-V.

50. Mackay A, Whittall K, Adler J, Li D, Paty D, Graeb D. In vivo visualization of myelin water

in brain by magnetic resonance. Magn. Reson. Med. 1994;31:673–677. doi: 10.1002/mrm.1910310614.

51. Webb S, Munro CA, Midha R, Stanisz GJ. Is multicomponent T2 a good measure of myelin content in peripheral nerve? Magn. Reson. Med. 2003;49:638–645. doi: 10.1002/mrm.10411.

52. Laule C, Leung E, Li DK, Traboulsee a L, Paty DW, Mackay a L, Moore GW. Myelin Water Imaging in Multiple Sclerosis : Quantitative Correlations with Histopathology. 2004;37:2004.

53. Laule C, Kozlowski P, Leung E, Li DKB, MacKay AL, Moore GRW. Myelin water imaging of multiple sclerosis at 7T: Correlations with histopathology. Neuroimage 2008;40:1575–1580. doi: 10.1016/j.neuroimage.2007.12.008.

54. MacKay A, Laule C, Vavasour I, Bjarnason T, Kolind S, M??dler B. Insights into brain microstructure from the T2 distribution. Magn. Reson. Imaging 2006;24:515–525. doi: 10.1016/j.mri.2005.12.037.

55. Whittall KP, MacKay AL. Quantitative interpretation of NMR relaxation data. J. Magn. Reson. 1989;84:134–152. doi: 10.1016/0022-2364(89)90011-5.

56. Lawson CL, Hanson RJ. Solving Least Squares Problems. 1974. doi: 10.1017/CBO9781107415324.004.

57. Laule C, Vavasour IM, Moore GRW, Oger J, Li DKB, Paty DW, MacKay a. L. Water content and myelin water fraction in multiple sclerosis. J. Neurol. 2004;251:284–293. doi: 10.1007/s00415-004-0306-6.

58. Vavasour IM, Whittall KP, Mackay AL, Li DKB, Vorobeychik G, Paty DW. A comparison between magnetization transfer ratios and myelin water percentages in normals and multiple sclerosis patients. Magn. Reson. Med. 1998;40:763–768. doi: 10.1002/mrm.1910400518.

59. Oakden W, Lobaugh N, Black S, Stanisz GJ. Quantitative T2 Relaxation of White Matter

Hyperintensities in Probable Alzheimer Patients. Int. Soc. Magn. Reson. Med. 2007;15:2146.

60. Flynn SW, Lang DJ, MacKay AL, et al. Abnormalities of myelination in schizophrenia detected in vivo with MRI, and post-mortem with analysis of oligodendrocyte proteins. Mol. Psychiatry 2003;8:811–820. doi: 10.1038/sj.mp.4001337.

61. Sirrs SMSM, Laule C, Madler B, et al. Normal-appearing White Matter in Patients with Phenylketonuria: Water Content, Myelin Water Fraction, and Metabolite Concentrations. Radiology 2007;242:236–243. doi: 242/1/236 [pii]\n10.1148/radiol.2421051758.

62. Moore GR, Leung E, MacKay a L, et al. A pathology-MRI study of the short-T2 component in formalin-fixed multiple sclerosis brain. Neurology 2000;55:1506–10. doi: 10.1212/WNL.55.10.1506.

63. Kozlowski P, Raj D, Liu J, Lam C, Yung AC, Tetzlaff W. Characterizing white matter damage in rat spinal cord with quantitative MRI and histology. J. Neurotrauma 2008;25:653–76. doi: 10.1089/neu.2007.0462.

64. D'Arceuil HE, Westmoreland S, de Crespigny AJ. An approach to high resolution diffusion tensor imaging in fixed primate brain. Neuroimage 2007;35:553–565. doi: 10.1016/j.neuroimage.2006.12.028.

65. McNab J a., Jbabdi S, Deoni SCL, Douaud G, Behrens TEJ, Miller KL. High resolution diffusion-weighted imaging in fixed human brain using diffusion-weighted steady state free precession. Neuroimage 2009;46:775–785. doi: 10.1016/j.neuroimage.2009.01.008.

66. Oguz KK, Kurne A, Aksu AO, Taskiran A, Karabulut E, Karabudak R. A comparative assessment of cerebral white matter by magnetization transfer imaging in early- and adult-onset multiple sclerosis patients matched for disease duration. J. Neurol. 2010;257:1309–1315. doi: 10.1007/s00415-010-5514-7.

67. Kolasinski J, Stagg CJ, Chance S a., et al. A combined post-mortem magnetic resonance imaging and quantitative histological study of multiple sclerosis pathology. Brain 2012;135:2938–2951. doi: 10.1093/brain/aws242.

68. Dyrby TB, Søgaard L V, Parker GJ, et al. Validation of in vitro probabilistic tractography. Neuroimage 2007;37:1267–77. doi: 10.1016/j.neuroimage.2007.06.022.

69. Burton JL, Underwood J. Clinical, educational, and epidemiological value of autopsy. Lancet 2007;369:1471–1480. doi: 10.1016/S0140-6736(07)60376-6.

70. Shojania KG, Burton EC, McDonald KM, Goldman L. Changes in rates of autopsy-detected diagnostic errors over time: a systematic review. JAMA 2003;289:2849–2856. doi: 10.1001/jama.289.21.2849\r289/21/2849 [pii].

71. Cannie M, Votino C, Moerman P, et al. Acceptance, reliability and confidence of diagnosis of fetal and neonatal virtuopsy compared with conventional autopsy: A prospective study. Ultrasound Obstet. Gynecol. 2012;39:659–665. doi: 10.1002/uog.10079.

72. Wichmann D, Obbelode F, Vogel H, Hoepker WW, Nierhaus A, Braune S, Sauter G, Pueschel K, Kluge S. Virtual autopsy as an alternative to traditional medical autopsy in the intensive care unit; A prospective cohort study. Ann. Intern. Med. 2012;156:123–130. doi: 10.7326/0003-4819-156-2-201201170-00008.

73. Thayyil S. Less invasive autopsy: an evidenced based approach. Arch. Dis. Child. 2011;96:681–687. doi: 10.1136/adc.2009.165704.

74. Kiernan J. Formaldehyde, formalin, paraformaldehyde and glutaraldehyde: what they are and what they do. Micros. Today 2000;12:8–12.

75. Thavarajah R, Mudimbaimannar VK, Elisabeth J, Rao UK, Ranganathan K. Chemical and physical basics of routine formaldehyde fixation. Journa Oral Maxxillofocial Pathol. 2012;16:400–

405. doi: 10.4103/0973-029X.102496.

76. Werner M, Chott A, Fabiano A, Battifora H. Effect of Formalin Tissue Fixation and Processing on Immunohistochemistry. Am. J. Surg. Pathol. 2000;24:1016–1019. doi: 10.1097/00000478-200007000-00014.

77. Tovi M, Ericsson A. Measurements of T1 and T2 over time in formalin-fixed human whole-brain specimens. Acta Radiol. 1992;33:400–4.

78. Yong-Hing CJ, Obenaus A, Stryker R, Tong K, Sarty GE. Magnetic resonance imaging and mathematical modeling of progressive formalin fixation of the human brain. Magn. Reson. Med. 2005;54:324–332. doi: 10.1002/mrm.20578.

79. Dawe RJ, Bennett D a, Schneider J a, Vasireddi SK, Arfanakis K. Postmortem MRI of human brain hemispheres: T2 relaxation times during formaldehyde fixation. Magn. Reson. Med. 2009;61:810–818. doi: 10.1002/mrm.21909.

80. McNab J a., Miller KL. Steady-state diffusion-weighted imaging: Theory, acquisition and analysis. NMR Biomed. 2010;23:781–793. doi: 10.1002/nbm.1509.

81. Van Duijn S, Nabuurs RJ a, Van Rooden S, Maat-Schieman MLC, Van Duinen SG, Van Buchem M a., Van Der Weerd L, Natté R. MRI artifacts in human brain tissue after prolonged formalin storage. Magn. Reson. Med. 2011;65:1750–1758. doi: 10.1002/mrm.22758.

82. Pfefferbaum A, Sullivan E V., Adalsteinsson E, Garrick T, Harper C. Postmortem MR imaging of formalin-fixed human brain. Neuroimage 2004;21:1585–1595. doi: 10.1016/j.neuroimage.2003.11.024.

83. Shepherd TM, Flint JJ, Thelwall PE, Stanisz GJ, Mareci TH, Yachnis AT, Blackband SJ. Postmortem interval alters the water relaxation and diffusion properties of rat nervous tissue--implications for MRI studies of human autopsy samples. Neuroimage 2009;44:820–6. doi:

10.1016/j.neuroimage.2008.09.054.

84. Matubayasi N, Nakahara M. Hydrothermal reactions of formaldehyde and formic acid: Free-energy analysis of equilibrium. J. Chem. Phys. 2005;122. doi: 10.1063/1.1849165.

85. Metz B. Identification of Formaldehyde-induced Modifications in Proteins: REACTIONS WITH MODEL PEPTIDES. J. Biol. Chem. 2003;279:6235–6243. doi: 10.1074/jbc.M310752200.

86. Madi S, Hasan KM, Narayana P a. Diffusion tensor imaging of in vivo and excised rat spinal cord at 7 T with an icosahedral encoding scheme. Magn. Reson. Med. 2005;53:118–125. doi: 10.1002/mrm.20304.

87. Sun SW, Neil JJ, Song SK. Relative indices of water diffusion anisotropy are equivalent in live and formalin-fixed mouse brains. Magn. Reson. Med. 2003;50:743–748. doi: 10.1002/mrm.10605.

88. Sun SW, Neil JJ, Liang HF, He YY, Schmidt RE, Hsu CY, Song SK. Formalin fixation alters water diffusion coefficient magnitude but not anisotropy in infarcted brain. Magn. Reson. Med. 2005;53:1447–1451. doi: 10.1002/mrm.20488.

89. Cynthia Mills DGS, Michael H. B, Amaral. Magnetic Resonance Imaging of the Post-Mortem Autistic Brain. J. Autism Dev. Disord. 2001;31:561–568.

90. Glutathione SOF, Nitric BY. Original Contribution. 2003;34:1078–1088. doi: 10.1016/S0891-5849(03)00038-8.

91. Mugler JP, Brookeman JR. Three-dimensional magnetization-prepared rapid gradient-echo imaging (3D MP RAGE). Magn. Reson. Med. 1990;15:152–157. doi: 10.1002/mrm.1910150117.

92. Nolte UG, Frahm J. Artifacts : Whole Brain Studies Using Diffusion-Weighted Single-Shot STEAM MR Imaging. 2000;736:731–736.

93. Bö L, Geurts J, Ravid R, Barkhof F. Magnetic resonance imaging as a tool to examine the neuropathology of multiple sclerosis. Neuropath. Appl. Neuro. 2004;30:106–117. doi:

10.1111/j.1365-2990.2004.00521.x.

94. Fox CH, Johnson FB, Whiting J, Roller PP. Formaldehyde fixation. J. Histochem. Cytochem. 1985;33:845–853. doi: 10.1177/33.8.3894502.

95. Turner R, Le Bihan D, Chesnick AS. Echo-planar imaging of diffusion and perfusion. Magn Reson Med 1991;19:247–53.

96. Marques JP, Kober T, Krueger G, van der Zwaag W, Van de Moortele PF, Gruetter R. MP2RAGE, a self bias-field corrected sequence for improved segmentation and T1-mapping at high field. Neuroimage 2010;49:1271–1281. doi: 10.1016/j.neuroimage.2009.10.002.

97. Ruthotto L, Kugel H, Olesch J, Fischer B, Modersitzki J, Burger M, Wolters CH. Diffeomorphic susceptibility artifact correction of diffusion-weighted magnetic resonance images. Phys. Med. Biol. 2012;57:5715–5731. doi: 10.1088/0031-9155/57/18/5715.

98. Murray ME, Vemuri P, Preboske GM, Murphy MC, Schweitzer KJ, Parisi JE, Jack CR, Dickson DW. A quantitative postmortem MRI design sensitive to white matter hyperintensity differences and their relationship with underlying pathology. J. Neuropathol. Exp. Neurol. 2012;71:1113–22. doi: 10.1097/NEN.0b013e318277387e.

99. Birkl C, Langkammer C, Golob-Schwarzl N, Leoni M, Haybaeck J, Goessler W, Fazekas F, Ropele S. Effects of formalin fixation and temperature on MR relaxation times in the human brain. NMR Biomed. 2016;29:458–465. doi: 10.1002/nbm.3477.

100. Broek JA, Guest PC, Rahmoune H, Bahn S. Proteomic analysis of post mortem brain tissue from autism patients: evidence for opposite changes in prefrontal cortex and cerebellum in synaptic connectivity-related proteins. Mol. Autism 2014;5:41. doi: 10.1186/2040-2392-5-41.

101. Langkammer C, Krebs N, Goessler W, Scheurer E, Ebner F, Yen K, Fazekas F, Ropele S. Quantitative MR Imaging of Brain Iron : A Postmortem Validation Study. Radiology

2010;257:455–462. doi: 10.1148/radiol.10100495.

102. Assaf Y, Pasternak O. Diffusion tensor imaging (DTI)-based white matter mapping in brain research: A review. J. Mol. Neurosci. 2008;34:51–61. doi: 10.1007/s12031-007-0029-0.

103. Barral JK, Gudmundson E, Stikov N, Etezadi-Amoli M, Stoica P, Nishimura DG. A robust methodology for in vivo T1 mapping. Magn. Reson. Med. 2010;64:1057–1067. doi: 10.1002/mrm.22497.

104. Lebel RM, Wilman AH. Transverse relaxometry with stimulated echo compensation. Magn. Reson. Med. 2010;64:1005–1014. doi: 10.1002/mrm.22487.

105. Uddin MN, Lebel RM, Wilman AH. Value of transverse relaxometry difference methods for iron in human brain. Magn. Reson. Imaging 2016;34:51–59. doi: 10.1016/j.mri.2015.09.002.

106. Sun H, Walsh AJ, Lebel RM, Blevins G, Catz I, Lu JQ, Johnson ES, Emery DJ, Warren KG, Wilman AH. Validation of quantitative susceptibility mapping with Perls' iron staining for subcortical gray matter. Neuroimage 2015;105:486–492. doi: 10.1016/j.neuroimage.2014.11.010.

107. Prasloski T, Rauscher A, MacKay AL, Hodgson M, Vavasour IM, Laule C, Mädler B. Rapid whole cerebrum myelin water imaging using a 3D GRASE sequence. Neuroimage 2012;63:533–539. doi: 10.1016/j.neuroimage.2012.06.064.

108. Shepherd TM, Thelwall PE, Stanisz GJ, Blackband SJ. Aldehyde fixative solutions alter the water relaxation and diffusion properties of nervous tissue. Magn. Reson. Med. 2009;62:26–34. doi: 10.1002/mrm.21977.

109. Birkl C, Langkammer C, Golob-Schwarzl N, Leoni M, Haybaeck J, Goessler W, Fazekas F, Ropele S. Effects of formalin fixation and temperature on MR relaxation times in the human brain. NMR Biomed. 2016. doi: 10.1002/nbm.3477.

110. Bottomley PA, Foster TH, Argersinger RE, Pfeifer LM. A review of normal tissue hydrogen

NMR relaxation times and relaxation mechanisms from 1–100 MHz: Dependence on tissue type, NMR frequency, temperature, species, excision, and age. Med. Phys. 1984;11:425–448. doi: 10.1118/1.595535.

111. Dusek P, Madai VI, Dieringer M, Hezel F, Niendorf T, Sobesky J, Matej R, Wuerfel J. Effect of embedding media on post-mortem MRI of formalin-fixed brain tissue at 7.0 T. Proc. Intl. Soc. Mag. Reson. Med. 22 1418. 2014;59:2014.

112. Bagnato F, Yao B, Cantor F, Merkle H, Condon E, Montequin M, Moore S, Quezado M, Tkaczyk D, McFarland H. Multisequence-imaging protocols to detect cortical lesions of patients with multiple sclerosis: Observations from a post-mortem 3 Tesla imaging study. J. Neurol. Sci. 2009;282:80–85. doi: 10.1016/j.jns.2009.03.021.

113. Oshio K, Feinberg D a. GRASE (Gradient- and spin-echo) imaging: a novel fast MRI technique. Magn. Reson. Med. 1991;20:344–349. doi: 10.1002/mrm.1910200219.

114. Ashburner J, Friston KJ. Unified segmentation. Neuroimage 2005;26:839–851. doi: 10.1016/j.neuroimage.2005.02.018.

115. Mohammadi S, Hutton C, Nagy Z, Josephs O, Weiskopf N. Retrospective correction of physiological noise in DTI using an extended tensor model and peripheral measurements. Magn. Reson. Med. 2013;70:358–369. doi: 10.1002/mrm.24467.

116. Mohammadi S, Freund P, Feiweier T, Curt A, Weiskopf N. The impact of post-processing on spinal cord diffusion tensor imaging. Neuroimage 2013;70:377–385. doi: 10.1016/j.neuroimage.2012.12.058.

117. Uddin MN, Marc Lebel R, Wilman AH. Transverse relaxometry with reduced echo train lengths via stimulated echo compensation. Magn. Reson. Med. 2013;70:1340–1346. doi: 10.1002/mrm.24568.

118. Hennig J. Multiecho imaging sequences with low refocusing flip angles. J. Magn. Reson. 1988;78:397–407. doi: 10.1016/0022-2364(88)90128-X.

119. Mazziotta JC, Toga AW, Evans A, Fox P, Lancaster J. A Probabilistic Atlas of the Human Brain: Theory and Rationale for Its Development. Neuroimage 1995;2:89–101. doi: 10.1006/nimg.1995.1012.

120. Beg MF, Miller MI, Trouve A, Younes L. Computing Large Deformation Metric Mappings via Geodesic Flows of Diffeomorphisms. Int. J. Comput. Vis. 2005;61:139–157.

121. Ceritoglu C, Oishi K, Li X, Chou MC, Younes L, Albert M, Lyketsos C, van Zijl PCM, Miller MI, Mori S. Multi-contrast large deformation diffeomorphic metric mapping for diffusion tensor imaging. Neuroimage 2009;47:618–627. doi: 10.1016/j.neuroimage.2009.04.057.

122. Faul F, Erdfelder E, Buchner A, Lang A-G. Statistical power analyses using G*Power 3.1: tests for correlation and regression analyses. Behav. Res. Methods 2009;41:1149–60. doi: 10.3758/BRM.41.4.1149.

123. Xie S, Zuo N, Shang L, Song M, Fan L, Jiang T. How does B-value affect HARDI reconstruction using clinical diffusion MRI data? PLoS One 2015;10. doi: 10.1371/journal.pone.0120773.

124. Kitajima M, Korogi Y, Takahashi M, Eto K. MR signal intensity of the optic radiation. Am. J. Neuroradiol. 1996;17:1379–1383.

125. Young IR, Hand JW, Oatridge A, Prior M V. Modeling and observation of temperature changes in vivo using MRI. Magn. Reson. Med. 1994;32:358–369. doi: 10.1002/mrm.1910320311.

126. Thickman DI, Kundel HL, Wolf G. Nuclear magnetic resonance characteristics of fresh and fixed tissue: the effect of elapsed time. Radiology 1983;148:183–185. doi:

10.1148/radiology.148.1.6856832.

127. Raman MR, Shu Y, Lesnick TG, Jack CR, Kantarci K. Regional T 1 relaxation time constants in Ex vivo human brain: Longitudinal effects of formalin exposure. Magn. Reson. Med. 2016;0:n/a-n/a. doi: 10.1002/mrm.26140.

128. Zhang Y, Moore GRW, Laule C, Bjarnason T a., Kozlowski P, Traboulsee A, Li DKB. Pathological correlates of magnetic resonance imaging texture heterogeneity in multiple sclerosis. Ann. Neurol. 2013;74:91–99. doi: 10.1002/ana.23867.

129. Cosgrove KP, Mazure CM, Staley JK. Evolving Knowledge of Sex Differences in Brain Structure, Function, and Chemistry. Biol. Psychiatry 2007;62:847–855. doi: 10.1016/j.biopsych.2007.03.001.

Appendix A

ELSEVIER LICENSE
TERMS AND CONDITIONS

Jan 23, 2017

This Agreement between Anwar Shahadat Shatil ("You") and Elsevier ("Elsevier") consists of your license details and the terms and conditions provided by Elsevier and Copyright Clearance Center.

License Number	4035010713263
License date	Jan 23, 2017
Licensed Content Publisher	Elsevier
Licensed Content Publication	Magnetic Resonance Imaging
Licensed Content Title	Insights into brain microstructure from the T2 distribution
Licensed Content Author	Alex MacKay,Cornelia Laule,Irene Vavasour,Thorarin Bjarnason,Shannon Kolind,Burkhard Mädler
Licensed Content Date	May 2006
Licensed Content Volume Number	24
Licensed Content Issue Number	4
Licensed Content Pages	11
Start Page	515
End Page	525
Type of Use	reuse in a thesis/dissertation
Portion	figures/tables/illustrations
Number of figures/tables/illustrations	2
Format	both print and electronic
Are you the author of this Elsevier article?	No
Will you be translating?	No
Order reference number	
Original figure numbers	Figure 1 and 2
Title of your thesis/dissertation	Quantitative MRI changes due to formalin fixation in whole ex vivo human brain specimens: Effects on diffusion anisotropy and diffusivity, T1 and T2 relaxation times, and multi-component myelin water fraction measurements at 3 T
Expected completion date	May 2017
Estimated size (number of pages)	70
Elsevier VAT number	GB 494 6272 12
Requestor Location	Anwar Shahadat Shatil Winnipeg, MB R3E 0M2

Canada
Attn: Anwar Shahadat Shatil

Total 0.00 CAD

Terms and Conditions

INTRODUCTION

1. The publisher for this copyrighted material is Elsevier. By clicking "accept" in connection with completing this licensing transaction, you agree that the following terms and conditions apply to this transaction (along with the Billing and Payment terms and conditions established by Copyright Clearance Center, Inc. ("CCC"), at the time that you opened your Rightslink account and that are available at any time at http://myaccount.copyright.com).

GENERAL TERMS

2. Elsevier hereby grants you permission to reproduce the aforementioned material subject to the terms and conditions indicated.
3. Acknowledgement: If any part of the material to be used (for example, figures) has appeared in our publication with credit or acknowledgement to another source, permission must also be sought from that source. If such permission is not obtained then that material may not be included in your publication/copies. Suitable acknowledgement to the source must be made, either as a footnote or in a reference list at the end of your publication, as follows:
"Reprinted from Publication title, Vol /edition number, Author(s), Title of article / title of chapter, Pages No., Copyright (Year), with permission from Elsevier [OR APPLICABLE SOCIETY COPYRIGHT OWNER]." Also Lancet special credit - "Reprinted from The Lancet, Vol. number, Author(s), Title of article, Pages No., Copyright (Year), with permission from Elsevier."
4. Reproduction of this material is confined to the purpose and/or media for which permission is hereby given.
5. Altering/Modifying Material: Not Permitted. However figures and illustrations may be altered/adapted minimally to serve your work. Any other abbreviations, additions, deletions and/or any other alterations shall be made only with prior written authorization of Elsevier Ltd. (Please contact Elsevier at permissions@elsevier.com). No modifications can be made to any Lancet figures/tables and they must be reproduced in full.
6. If the permission fee for the requested use of our material is waived in this instance, please be advised that your future requests for Elsevier materials may attract a fee.
7. Reservation of Rights: Publisher reserves all rights not specifically granted in the combination of (i) the license details provided by you and accepted in the course of this licensing transaction, (ii) these terms and conditions and (iii) CCC's Billing and Payment terms and conditions.
8. License Contingent Upon Payment: While you may exercise the rights licensed immediately upon issuance of the license at the end of the licensing process for the transaction, provided that you have disclosed complete and accurate details of your proposed use, no license is finally effective unless and until full payment is received from you (either by publisher or by CCC) as provided in CCC's Billing and Payment terms and conditions. If full payment is not received on a timely basis, then any license preliminarily granted shall be deemed automatically revoked and shall be void as if never granted. Further, in the event that you breach any of these terms and conditions or any of CCC's Billing and Payment terms and conditions, the license is automatically revoked and shall be void as if never granted. Use of materials as described in a revoked license, as well as any use of the materials beyond the scope of an unrevoked license, may constitute copyright infringement and publisher reserves the right to take any and all action to protect its copyright in the materials.
9. Warranties: Publisher makes no representations or warranties with respect to the licensed material.

10. Indemnity: You hereby indemnify and agree to hold harmless publisher and CCC, and their respective officers, directors, employees and agents, from and against any and all claims arising out of your use of the licensed material other than as specifically authorized pursuant to this license.
11. No Transfer of License: This license is personal to you and may not be sublicensed, assigned, or transferred by you to any other person without publisher's written permission.
12. No Amendment Except in Writing: This license may not be amended except in a writing signed by both parties (or, in the case of publisher, by CCC on publisher's behalf).
13. Objection to Contrary Terms: Publisher hereby objects to any terms contained in any purchase order, acknowledgment, check endorsement or other writing prepared by you, which terms are inconsistent with these terms and conditions or CCC's Billing and Payment terms and conditions. These terms and conditions, together with CCC's Billing and Payment terms and conditions (which are incorporated herein), comprise the entire agreement between you and publisher (and CCC) concerning this licensing transaction. In the event of any conflict between your obligations established by these terms and conditions and those established by CCC's Billing and Payment terms and conditions, these terms and conditions shall control.
14. Revocation: Elsevier or Copyright Clearance Center may deny the permissions described in this License at their sole discretion, for any reason or no reason, with a full refund payable to you. Notice of such denial will be made using the contact information provided by you. Failure to receive such notice will not alter or invalidate the denial. In no event will Elsevier or Copyright Clearance Center be responsible or liable for any costs, expenses or damage incurred by you as a result of a denial of your permission request, other than a refund of the amount(s) paid by you to Elsevier and/or Copyright Clearance Center for denied permissions.

LIMITED LICENSE

The following terms and conditions apply only to specific license types:
15. **Translation**: This permission is granted for non-exclusive world **English** rights only unless your license was granted for translation rights. If you licensed translation rights you may only translate this content into the languages you requested. A professional translator must perform all translations and reproduce the content word for word preserving the integrity of the article.
16. **Posting licensed content on any Website**: The following terms and conditions apply as follows: Licensing material from an Elsevier journal: All content posted to the web site must maintain the copyright information line on the bottom of each image; A hyper-text must be included to the Homepage of the journal from which you are licensing at http://www.sciencedirect.com/science/journal/xxxxx or the Elsevier homepage for books at http://www.elsevier.com; Central Storage: This license does not include permission for a scanned version of the material to be stored in a central repository such as that provided by Heron/XanEdu.
Licensing material from an Elsevier book: A hyper-text link must be included to the Elsevier homepage at http://www.elsevier.com . All content posted to the web site must maintain the copyright information line on the bottom of each image.

Posting licensed content on Electronic reserve: In addition to the above the following clauses are applicable: The web site must be password-protected and made available only to bona fide students registered on a relevant course. This permission is granted for 1 year only. You may obtain a new license for future website posting.
17. **For journal authors:** the following clauses are applicable in addition to the above:
Preprints:
A preprint is an author's own write-up of research results and analysis, it has not been peer-reviewed, nor has it had any other value added to it by a publisher (such as formatting, copyright, technical enhancement etc.).

Authors can share their preprints anywhere at any time. Preprints should not be added to or enhanced in any way in order to appear more like, or to substitute for, the final versions of articles however authors can update their preprints on arXiv or RePEc with their Accepted Author Manuscript (see below).
If accepted for publication, we encourage authors to link from the preprint to their formal publication via its DOI. Millions of researchers have access to the formal publications on ScienceDirect, and so links will help users to find, access, cite and use the best available version. Please note that Cell Press, The Lancet and some society-owned have different preprint policies. Information on these policies is available on the journal homepage.
Accepted Author Manuscripts: An accepted author manuscript is the manuscript of an article that has been accepted for publication and which typically includes author-incorporated changes suggested during submission, peer review and editor-author communications.
Authors can share their accepted author manuscript:

- immediately
    - via their non-commercial person homepage or blog
    - by updating a preprint in arXiv or RePEc with the accepted manuscript
    - via their research institute or institutional repository for internal institutional uses or as part of an invitation-only research collaboration work-group
    - directly by providing copies to their students or to research collaborators for their personal use
    - for private scholarly sharing as part of an invitation-only work group on commercial sites with which Elsevier has an agreement
- after the embargo period
    - via non-commercial hosting platforms such as their institutional repository
    - via commercial sites with which Elsevier has an agreement

In all cases accepted manuscripts should:

- link to the formal publication via its DOI
- bear a CC-BY-NC-ND license - this is easy to do
- if aggregated with other manuscripts, for example in a repository or other site, be shared in alignment with our hosting policy not be added to or enhanced in any way to appear more like, or to substitute for, the published journal article.

Published journal article (JPA): A published journal article (PJA) is the definitive final record of published research that appears or will appear in the journal and embodies all value-adding publishing activities including peer review co-ordination, copy-editing, formatting, (if relevant) pagination and online enrichment.
Policies for sharing publishing journal articles differ for subscription and gold open access articles:
Subscription Articles: If you are an author, please share a link to your article rather than the full-text. Millions of researchers have access to the formal publications on ScienceDirect, and so links will help your users to find, access, cite, and use the best available version.
Theses and dissertations which contain embedded PJAs as part of the formal submission can be posted publicly by the awarding institution with DOI links back to the formal publications on ScienceDirect.
If you are affiliated with a library that subscribes to ScienceDirect you have additional private sharing rights for others' research accessed under that agreement. This includes use for classroom teaching and internal training at the institution (including use in course packs and courseware programs), and inclusion of the article for grant funding purposes.
Gold Open Access Articles: May be shared according to the author-selected end-user license and should contain a CrossMark logo, the end user license, and a DOI link to the

formal publication on ScienceDirect.
Please refer to Elsevier's posting policy for further information.
18. **For book authors** the following clauses are applicable in addition to the above: Authors are permitted to place a brief summary of their work online only. You are not allowed to download and post the published electronic version of your chapter, nor may you scan the printed edition to create an electronic version. **Posting to a repository:** Authors are permitted to post a summary of their chapter only in their institution's repository.
19. **Thesis/Dissertation**: If your license is for use in a thesis/dissertation your thesis may be submitted to your institution in either print or electronic form. Should your thesis be published commercially, please reapply for permission. These requirements include permission for the Library and Archives of Canada to supply single copies, on demand, of the complete thesis and include permission for Proquest/UMI to supply single copies, on demand, of the complete thesis. Should your thesis be published commercially, please reapply for permission. Theses and dissertations which contain embedded PJAs as part of the formal submission can be posted publicly by the awarding institution with DOI links back to the formal publications on ScienceDirect.

Elsevier Open Access Terms and Conditions
You can publish open access with Elsevier in hundreds of open access journals or in nearly 2000 established subscription journals that support open access publishing. Permitted third party re-use of these open access articles is defined by the author's choice of Creative Commons user license. See our open access license policy for more information.
Terms & Conditions applicable to all Open Access articles published with Elsevier:
Any reuse of the article must not represent the author as endorsing the adaptation of the article nor should the article be modified in such a way as to damage the author's honour or reputation. If any changes have been made, such changes must be clearly indicated.
The author(s) must be appropriately credited and we ask that you include the end user license and a DOI link to the formal publication on ScienceDirect.
If any part of the material to be used (for example, figures) has appeared in our publication with credit or acknowledgement to another source it is the responsibility of the user to ensure their reuse complies with the terms and conditions determined by the rights holder.
Additional Terms & Conditions applicable to each Creative Commons user license:
CC BY: The CC-BY license allows users to copy, to create extracts, abstracts and new works from the Article, to alter and revise the Article and to make commercial use of the Article (including reuse and/or resale of the Article by commercial entities), provided the user gives appropriate credit (with a link to the formal publication through the relevant DOI), provides a link to the license, indicates if changes were made and the licensor is not represented as endorsing the use made of the work. The full details of the license are available at http://creativecommons.org/licenses/by/4.0.
CC BY NC SA: The CC BY-NC-SA license allows users to copy, to create extracts, abstracts and new works from the Article, to alter and revise the Article, provided this is not done for commercial purposes, and that the user gives appropriate credit (with a link to the formal publication through the relevant DOI), provides a link to the license, indicates if changes were made and the licensor is not represented as endorsing the use made of the work. Further, any new works must be made available on the same conditions. The full details of the license are available at http://creativecommons.org/licenses/by-nc-sa/4.0.
CC BY NC ND: The CC BY-NC-ND license allows users to copy and distribute the Article, provided this is not done for commercial purposes and further does not permit distribution of the Article if it is changed or edited in any way, and provided the user gives appropriate credit (with a link to the formal publication through the relevant DOI), provides a link to the license, and that the licensor is not represented as endorsing the use made of the work. The full details of the license are available at http://creativecommons.org/licenses/by-nc-nd/4.0.
Any commercial reuse of Open Access articles published with a CC BY NC SA or CC BY NC ND license requires permission from Elsevier and will be subject to a fee.

Commercial reuse includes:

- Associating advertising with the full text of the Article
- Charging fees for document delivery or access
- Article aggregation
- Systematic distribution via e-mail lists or share buttons

Posting or linking by commercial companies for use by customers of those companies.

20. **Other Conditions**:

v1.9